


Reassessing evidence of Moon–Earth dynamics from tidal bundles at 3.2 Ga (Moodies Group, Barberton Greenstone Belt, South Africa)

CHRISTOPH HEUBECK* , SASKIA BLÄSING†, NADJA DRABON‡, TOM EULENFELD*, MARC ULRICH GRUND†, MARTIN HOMANN§, DEON JANSE VAN RENSBURG*, INGA KÖHLER*¹, SAMI NABHAN*², CAROLIN RABETHGE†, THOMAS VOIGT* and DANIELLE ZENTNER-JOERGES¶

*Institut für Geowissenschaften, Friedrich-Schiller-Universität Jena, Burgweg 11, Jena, 07749, Germany (E-mail: christoph.heubeck@uni-jena.de)

†Institut für Geologische Wissenschaften, FU Berlin, Malteserstr. 74-100, Berlin, 12249, Germany

‡Dept. of Earth and Planetary Sciences, Harvard University, Cambridge, MA, 02138, USA

§Department of Earth Sciences, University College London, London, WC1E 6BT, UK

¶Department of Geological Sciences, Stanford University, Stanford, CA, 94305, USA

Associate Editor – Nicholas Tosca

ABSTRACT

Past orbital parameters of the Moon are difficult to reconstruct from geological records because relevant data sets of tidal strata are scarce or incomplete. The sole Archean data point is from the Moodies Group (*ca* 3.22 Ga) of the Barberton Greenstone Belt, South Africa. From the time-series analysis of tidal bundles from a well-exposed subaqueous sand wave of this unit, Eriksson and Simpson (*Geology*, 28, 831) suggested that the Moon's anomalistic month at 3.2 Ga was closer to 20 days than the present 27.5 days. This is in apparent accordance with models of orbital mechanics which place the Archean Moon in a closer orbit with a shorter period, resulting in stronger tidal action. Although this study's detailed geological mapping and section measuring of the site confirmed that the sandstone bed in question is likely a migrating dune, the presence of angular mud clasts, channel-margin slumps, laterally aggrading channel fills and bidirectional paleocurrents in overlying and underlying beds suggests that this bedform was likely located in a nearshore channel near lower-intertidal flats and subtidal estuarine bars; it thus carries risk of incomplete preservation. Repeated measurements of foreset thicknesses along the published traverse, measured perpendicular to bedding, failed to show consistent spectral peaks. Larger data sets acquired along traverses measured parallel to bedding along the 20.5 m wide exposure are affected by minor faulting, uneven outcrop weathering, changing illumination, weather, observer bias and show a low reproducibility. The most robust measurements herein confirm the periodicity peak of approximately 14 in the original data of Eriksson and Simpson (*Geology*, 28, 831). Because laminae may have been eroded, the measurements may represent a lower bound of about 28 lunar days per synodic month. This estimate agrees well with Earth–Moon dynamic models which consider the conservation of angular momentum and place the Archaean Moon in a lower orbit around a faster-spinning Earth.

¹Present address: Am Feldrain 2, Altenmünster, 97488

²Present address: Department of Biology, Nordcee, University of Southern Denmark, Campusvej 55, 5230 Odense, Odense, 5230, Denmark

Keywords Archean, Barberton Greenstone Belt, Earth–Moon distance, Earth–Moon dynamics, Moodies Group, tidal sedimentation, time-series analysis.

INTRODUCTION

Knowledge of the dynamics and parameters governing Archean tides can be used to reconstruct the interaction of the Earth–Moon system. Little is known, however, about the role of tides in the earliest rock record (Williams, 1990, 2000, 2004; Kagan, 1997; Coughenour *et al.*, 2009; Eriksson *et al.*, 2013). Knowledge about the relationship between the Moon and tides has been growing exponentially (see, for reviews, e.g., Smith *et al.*, 1991; Sonett *et al.*, 1996; Kagan, 1997; Coughenour *et al.*, 2009; Green *et al.*, 2017). Ever since Apollo Lunar Laser Ranging established that the Moon's orbit about Earth currently grows at a rate of about 3.8 cm year^{-1} (the so-called lunar recession rate; Dickey *et al.*, 1994), attempts have been made to quantitatively reconstruct the dynamics of the Earth–Moon system in 'deep time'. Because the Moon would be impossibly young (only about 1.5 Gyr old) if the present lunar recession rate had been constant throughout Earth's history, the recession rate must have been significantly lower in the geological past (Lambeck, 1980; Sonett *et al.*, 1996; Kvale *et al.*, 1997, 1999; Bills & Ray, 1999; Williams, 2000; Coughenour *et al.*, 2009; Lopez de Azarevich & Azarevich, 2017).

The transfer of angular momentum from Earth to Moon which acts to slow down the orbital velocity of the Moon and increases its orbital radius is, in first approximation, a function of the tidal friction (also termed 'tidal dissipation'; Lambeck, 1980; Brosche, 1984; Coughenour *et al.*, 2009; Tyler, 2021), which also slows down Earth's rotation (spin). This tidal friction is largely exerted through tidal currents moving over the seabed; it is thus a complex function of the world's (mostly shallow) oceanic areas and continental configuration which is poorly constrained through deep time (see, e.g., Sündermann & Brosche, 1978; Hansen, 1982; Tyler, 2021). Thus, the reconstruction of the Moon's orbit is fraught with uncertainty (see, e.g., Kagan & Sündermann, 1996; Bills & Ray, 1999; Kvale *et al.*, 1999; Lopez de Azarevich & Azarevich, 2017). It is probably safe to assume, however,

that the Moon circled Earth in a lower orbit in the distant past, that its orbital period consequently was shorter and that the gravitational attraction of the Moon on Earth's oceans was stronger (Kvale *et al.*, 1999; Williams, 2000; Mazumder, 2005; Coughenour *et al.*, 2009; Tyler, 2021).

Because the global distribution of frequency and amplitude of recent tides (none to three times daily; 0 to 18 m) depends less on secular astronomical parameters than on local controls, such as coastal topography, nearshore bathymetry, wind patterns and ocean basin geometry, preserved tidal evidence may have limited value to reconstruct global parameters (Kvale, 2006; Longhitano *et al.*, 2012, and many others). Palaeontological records based on growth strata are commonly ambiguous and rarely exist beyond the Cambrian (Lambeck, 1980; Vanyo & Awramik, 1985; Richardson, 1990; Sonett *et al.*, 1996). Only a tiny fraction of Archean time was recorded and preserved in very few, small and fragmentary rock records. Thus, reconstructions of Archean tidal dynamics are rare. The few existing Archean rock records of tidal action should therefore be examined with particular interest and care.

Precambrian tidal strata are common but quantitative records documenting lunar tidal forcing are very rare. For the Proterozoic estimates of lunar periodicities, some with considerable uncertainties and likely large errors on quantitative calculations, appear to exist from five geological units; the Neoproterozoic Elatina Rhythmites of South Australia (*ca* 620 Ma; Williams, 1991); the Cryogenian of Scotland (*ca* 660 Ma; Kessler & Gollop, 1988); the Neoproterozoic to Mesoproterozoic Big Cottonwood Formation of Utah, USA (*ca* 850 to 1100 Ma; Chan *et al.*, 1994; Sonett & Chan, 1998); the Palaeoproterozoic Chaibasa tidal rhythmite of India (*ca* 2.2 Ga; Mazumder, 2004; Mallik *et al.*, 2012); and the Palaeoproterozoic Weeli Wolli banded-iron-formation of West Australia (*ca* 2450 Ma; Trendall, 1973; Williams, 2000). Although the latter example may not represent a tidal deposit and most data sets are plagued by

either short records and/or incomplete preservation, they indicate a decreasing number of lunar months per year, a decreasing number of days per year and an increasing Earth–Moon distance with time (Williams, 2000, 2004; Eriksson *et al.*, 2013). For the Archean Eon (4.0 to 2.5 Ga), a single data point exists from the Moodies Group of South Africa's and Eswatini's Barberton Greenstone Belt (BGB; *ca* 3.22 Ga; Zeh *et al.*, 2013; Byerly *et al.*, 2018; Fig. 1). In an analysis of the rhythmic variations of foreset thicknesses of a large, very well-exposed subaquatic sand dune from the best-suited outcrop of this unit, Eriksson & Simpson (2000) removed the record of the subordinate tide of an assumed semidiurnal (twice daily) tidal signal, leaving them with the diurnal record (De Boer *et al.*, 1989). After spectral (time-series) analysis of the reduced data set, they interpreted the remaining peak periodicity of 9.3 as reflecting a spring–neap–spring cycle between New Moon and Full Moon (half a synodic period) and thus inferred a synodic month of approximately twice that number in lunar days, compared to 29 days 13 h at

present (Kvale *et al.*, 1999; Kvale, 2006; Coughenour *et al.*, 2009). The present study reports on the re-examination of this outcrop and compares its data with the data set of Eriksson & Simpson (2000).

REGIONAL GEOLOGY

The Moodies Group of the Barberton Greenstone Belt, South Africa and Eswatini, is one of the oldest well-preserved siliciclastic shallow-water units on Earth (Visser *et al.*, 2012; Anhaeusser, 1976; Eriksson, 1979; Heubeck, 2019). It reaches up to 3.7 km thick and occurs over an area approximately 40 by 70 km. The unit constitutes the uppermost part of the Barberton Supergroup and is generally exposed in large, tightly folded and steeply plunging, north-east/south-west-trending synclines up to 15 km long and several kilometres wide (Anhaeusser, 1976; Lowe *et al.*, 2012; Schmitz & Heubeck, 2021; Fig. 1). Most strata show subvertical dips. Despite the large-scale folding and several phases of alteration

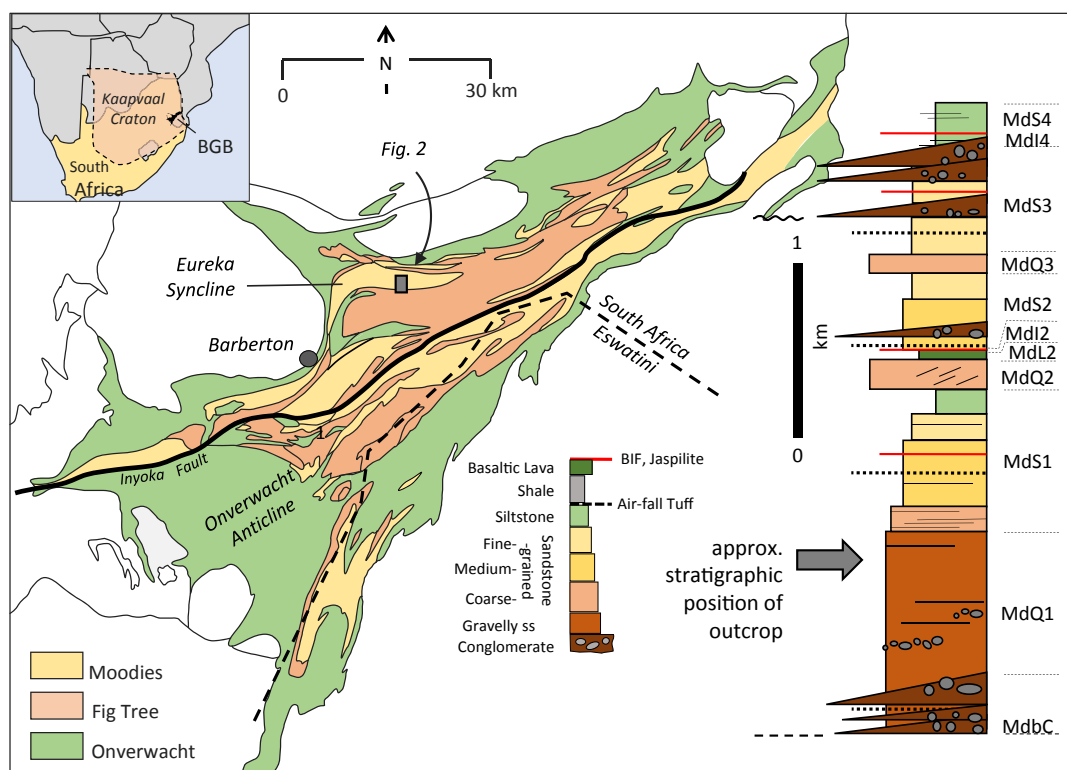


Fig. 1. Generalized geological map of the Barberton Greenstone Belt (BGB) in South Africa and Eswatini. Inset map shows location of the BGB at the eastern margin of the Kaapvaal Craton of southern Africa. Stratigraphic column shows generalized stratigraphy of the Moodies Group, uppermost unit of the greenstone belt fill. Small grey rectangle marks location of the geological map of the study area in Fig. 2.

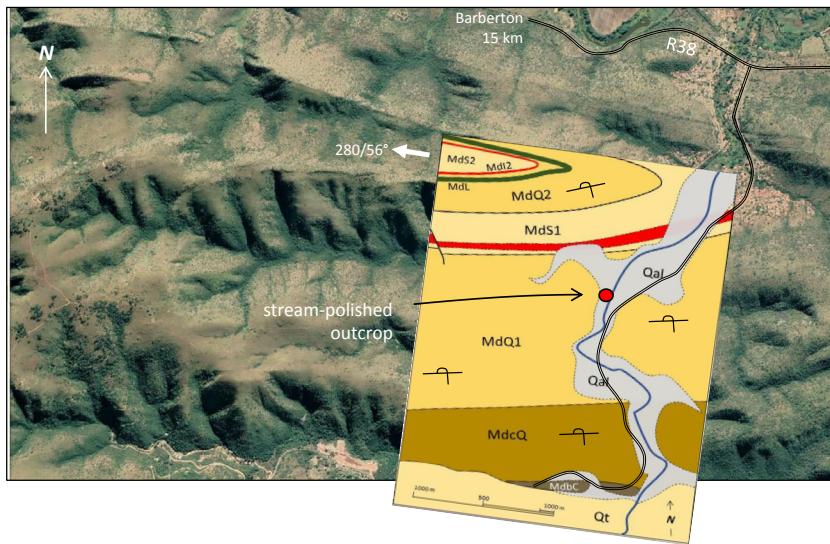


Fig. 2. Google Earth© Image of the eastern Eureka Syncline of the Barberton Greenstone Belt; the inset geological map shows generalized geology along Fig Tree Creek. Stratigraphic abbreviations follow Anhaeusser (1976). The outcrop (red circle) lies within thick tidal-facies quartzose sandstones of unit MdQ1 on the overturned southern limb of the Eureka Syncline. Strata in this limb dip steeply south and face northward.

and metamorphism, metamorphic grade is at lower greenschist facies (Xie *et al.*, 1997; Toulkeridis *et al.*, 1998); penetrative strain, except close to fold axes and major fault zones, is low to nil (Anhaeusser, 1976; Schmitz & Heubeck, 2021).

Moodies Group strata consist mostly of quartz-rich sandstones, with subordinate siltstones, conglomerates and shales as well as minor BIF (banded iron formation), jaspilite, and volcanic rocks which were largely deposited in fluvial, shoreline, tidal and deltaic settings (Eriksson, 1977, 1979; Heubeck & Lowe, 1994a, 1994b; Heubeck *et al.*, 2013, 2016; Homann *et al.*, 2015; Nabhan *et al.*, 2016; Heubeck, 2019; Stutenbecker *et al.*, 2019; Reimann *et al.*, 2021). Deep-water, below-wave base deposits, mostly in prodelta-facies, are common but poorly exposed; alluvial environments are restricted to the base and the top of the unit. Despite their considerable thickness, Moodies Group strata were likely deposited within only *ca* 1 to 10 Ma between approximately 3224 Ma and 3214 Ma (Heubeck *et al.*, 2013, 2022). The overall mean depositional rate was approximately 0.1 to 1.0 mm a⁻¹, comparable with many Holocene depositional rates at passive margins. After considering for local cryptic disconformities and hiatuses, actual depositional rates could have been substantially higher. Conditions were thus regionally and temporally favourable to record a very-high-resolution record of Archean coastal processes.

Moodies Group strata are well-exposed throughout the BGB, for example in the

prominent, boomerang-shaped Eureka Syncline. Approximately 15 km north-east of Barberton, the Eureka Syncline is traversed approximately at right angle to bedding by the northward-draining Fig Tree Creek (Fig. 2; Anhaeusser, 1976; Eriksson, 1977), exposing a *ca* 1300 m thick section of cross-bedded sandstones (unit MdQ1 of Anhaeusser, 1976) on the overturned southern limb of Eureka Syncline, in part in very-well-exposed stream-polished plates and low cliffs. Above a basal gravelly and tuffaceous sandstone section in fluvial–braidplain facies, the section is dominated by cross-bedded and horizontally bedded, quartzose, medium-grained, well-sorted and quartz–sericite-cemented feldspathic sublitharenites; see Heubeck & Lowe (1999) and Reimann *et al.* (2021) for a petrographic description of Moodies sandstones. Bedsets are commonly separated from each other by shallow scour surfaces and more rarely by millimetre-thin to centimetre-thin, dark grey, fine-sandy chloritic siltstones. Uncommon well-rounded chert pebbles, shale rip-up clasts and shale drapes on rippled surfaces attest to variable flow velocities. There are no indications of major scours or of erosional downcutting. The geometry of the abundant sedimentary structures and thin-section petrography show that compaction was minor and that carbonate, clay (now sericite) and silica cementation occurred in many places early-diagenetically (Heubeck & Lowe, 1999; Reimann *et al.*, 2021).

In the streambed of Fig Tree Creek, Eriksson & Simpson (2000) studied a sandstone bed *ca* 1.0



Fig. 3. Panoramic photographs of streambedded outcrop in Fig Tree Creek showing the subaquatic tidal dune (unit J) of Eriksson & Simpson (2000) discussed in this paper. (A) View westward across Fig Tree Creek (foreground). Beds strike east–west, dip steeply south and face north. Outcrop is *ca* 20.5 m long and *ca* 20.5 m wide. Letters denote stratigraphic units shown in the stratigraphic column (Fig. 6) and the geological map (Fig. 7). (B) View upstream (stratigraphically downsection) along Fig Tree Creek. The investigated outcrop shown in Fig. 3A consists of the tilted rock face in the centre and right foreground.

to 1.2 m thick which is exposed over 20.5 m length between a low vegetated cliff and Fig Tree Creek (Figs 3 to 5). This bed consists wholly of foresets. Each foreset consists of a thin sandstone bed separated by a sub-millimetre-thin mudstone lamina; each sandstone–mudstone couplet forms a ‘bundle’. Geochemical analyses from other outcrops (Hessler & Lowe, 2006) show that shale laminae consist of a very-fine-grained mix of chlorite-group clay minerals, quartz, sericite, and minor carbonate and opaque organic matter. In thin section, the laminae can be seen draping topmost sand grains of the underlying sandstone bed.

Eriksson & Simpson (2000) interpreted these foreset laminae to have formed by periodic

activation of sand transport on a subtidal sand wave by tidal currents; they interpreted their varying thicknesses as reflecting the varying strength of tidal rhythmicity due to an astronomically forced semidiurnal tide (Allen, 1982; Yang & Nio, 1985; de Boer *et al.*, 1989; Archer, 1996; Friedman & Chakraborty, 2006).

In this pattern, a thinner bundle (Dalrymple, 1992; Friedman *et al.*, 1992; Friedman & Chakraborty, 2006) represented the daily subordinate tide, the following thicker bundle the dominant tide. Fourier analysis on a reduced data set measured along a single traverse perpendicular to bedding (Traverse 2A of Eriksson & Simpson, 2000) showed thickening–thinning–thickening trends, each nine or ten bundles thick. Eriksson

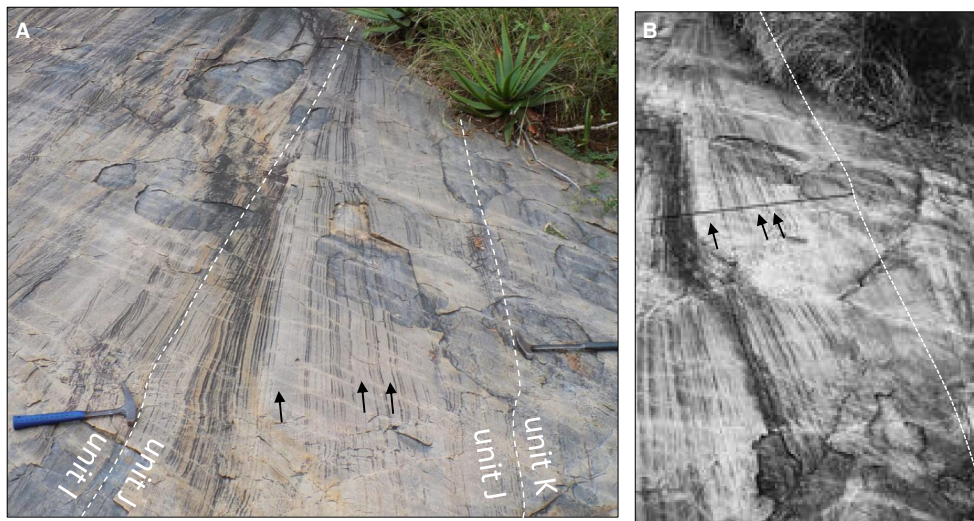


Fig. 4. Comparison of outcrop conditions in 2021 (Fig. 4A) to those shown in Eriksson & Simpson (2000, fig. 2; reproduced in Fig. 4B). Section measured by Eriksson & Simpson (2000) lies between the tops of the geology picks shown in Fig. 4A and is marked by the black line shown in Fig. 4B. Black arrows indicate three thick bundle sets recognizable in both outcrop photographs. They are also well-represented in the histogram of laminae thicknesses (Fig. 9). Hammer to the left in (A) is 28 cm, hammer to the right 40 cm long. Traverse line in (B) is ca 1 m long.

& Simpson (2000) interpreted these as spring–neap–spring cycles and thus inferred (incorrectly) the anomalistic month (presently 27 days 13 h) to have been of 18 to 21 days duration; correct would have been to infer the duration of the synodic month, currently 29 days 13 h (Nio & Yang, 1991; Archer, 1996; Friedman & Chakraborty, 2006).

METHODS

This study first mapped exposures of the ca 1.4 km thick Moodies Group along Fig Tree Creek, then mapped the outcrop stratigraphically, recording lithologies and sedimentary structures, and measured a section along the centre of the outcrop. Particular attention was directed to unit J (Figs 4 and 5). In this unit, Eriksson & Simpson (2000) had measured “along two traverses through the cross-bed set perpendicular to master bedding” but showed and discussed results of Traverse 2 only (their fig. 2); this traverse can be precisely identified in outcrop (Fig. 4). The present study remeasured apparent couplet thicknesses along this traverse, defined as the distance between midpoints of adjacent shale laminae perpendicular to the strike of the laminae because shale laminae are consistently much thinner (significantly less than a millimetre) than the interspersed sand beds.

Our measurements were made three times and not more than a few centimetres from the original location of Traverse 2: In 2014 on the wet and on the dry rock face, and again in 2021, assuming that Eriksson & Simpson’s (2000) original Traverse 2 had been measured base-to-top. Realizing the limitations of traverses perpendicular to bedding and recognizing that measuring along strike could yield a significantly larger data set, Eriksson & Simpson (2000) also “measured along one traverse through the middle of the cross-bed set parallel to master bedding” of unit J where foreset laminae are well-developed and largely continuous; they did not present data nor discuss results. Because the authors agree that such an acquisition strategy would be better suited to avoid the effects of topset slumping and lee–eddy backwash, their approach was taken up in two variations:

1 Traverses were measured in three teams and under varying conditions along a taut string strung approximately midway the preserved dune height, that is, about 50 cm above its base. Thereby, significantly larger data sets (up to 337 values) were obtained along ca 18 m outcrop length.

2 The published data set of Eriksson & Simpson (2000) was enlarged by remeasuring their traverse and then tracing a bottomset of this traverse along strike into a topset a few metres up-current where a new traverse was measured.

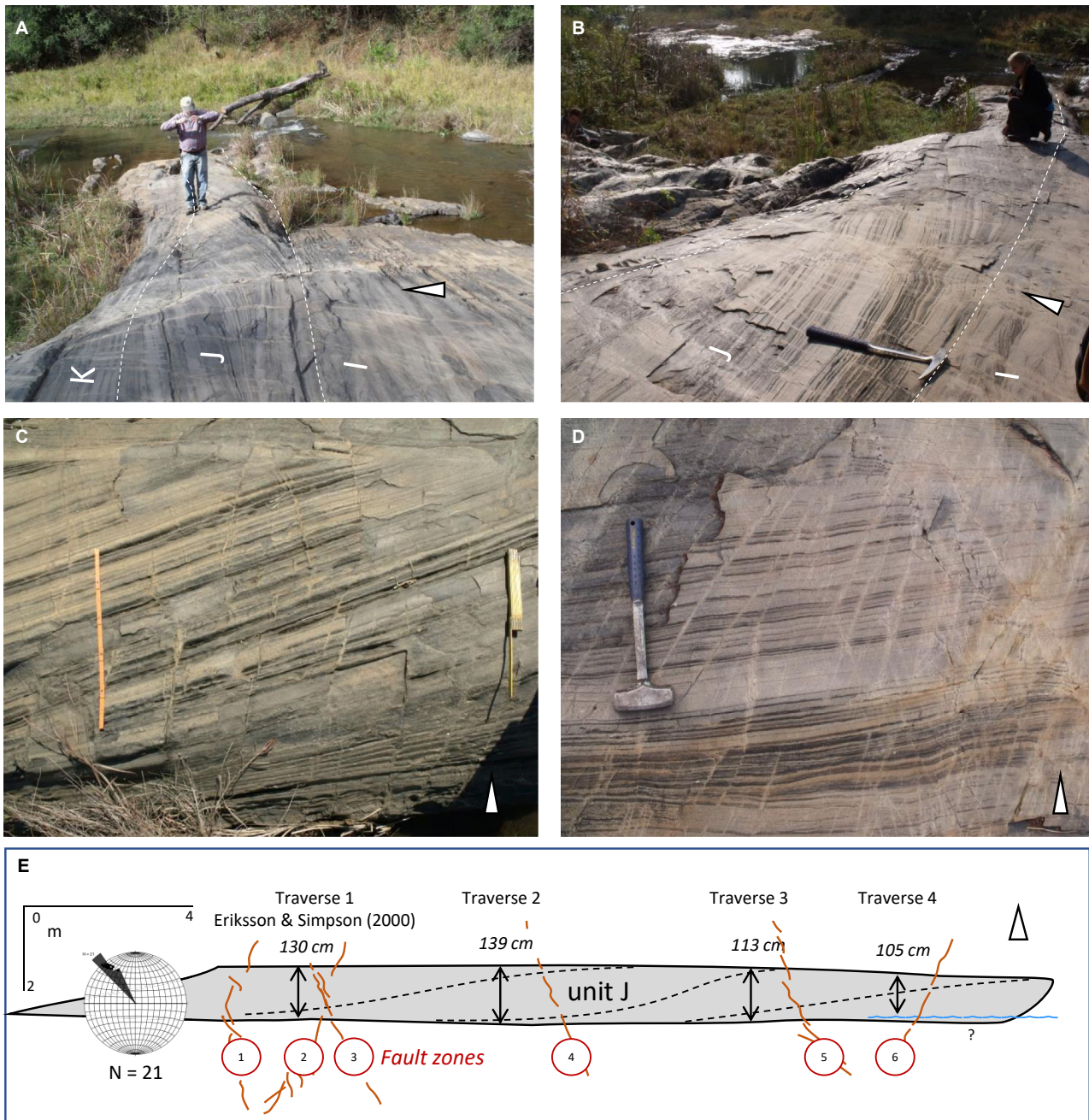


Fig. 5. Outcrop photographs and sketch of unit J. White triangles indicate stratigraphic-up direction. (A) Photograph from July, 2013. Apparent migration direction of the dune (unit J) is towards the viewer. Person for scale. Unit J is *ca* 1 m thick. (B) View along strike to the east; hammer is 40 cm long. (C) and (D) Foreset laminae of unit J. Foreset laminae of different thicknesses are clustered but a rhythmic pattern is not clearly apparent. Foldout scale [right in (C)] is 40 cm long; hammer in (D) is 41 cm long. (E) Sketch of unit J. Outcrop width is 20.5 m; bed thickness varies between *ca* 105 cm and 140 cm. Red lines indicate approximate positions of minor faults and fracture zones; dashed black lines show foresets used to correlate between Traverses 1 through to 4 (cp. Fig. 13).

Repeating this approach, a composite data set of 224 bundle thicknesses was generated from four correlated traverses. In all measurement

sessions, readers took care not to allow their readings be affected by biases developing during the measuring process.

Data sets were annotated, plotted and analyzed using the FFT (fast Fourier transform) algorithm implemented in Scipy (Virtanen *et al.*, 2020). Data were not selectively removed, as Eriksson & Simpson (2000) had done in order to conform to the assumption of a minor semidiurnal tide. The approach of digital image analysis of foreset thicknesses proved inefficient and ambiguous due to artifacts of changing illumination and varying degrees of weathering.

Palaeotransport directions were calculated from nearly all units of this outcrop using the software STERONET 10.0 (Allmendinger *et al.*, 2011; Cardozo & Allmendinger, 2013). Sedimentary bedding is oriented *ca* 190/74°. This study corrected for the structural orientation of the strata on the limb of a plunging syncline (Figs 1 and 2) by rotating the lines representing foreset dip directions and dips (for example, 187/63) +65° about an axis with azimuth 010 and plunge 0°, then by restoring the overturned bedding to the horizontal by rotating −106° about an axis with azimuth 280 and plunge 0°. Foreset dip directions and dip angles were plotted on rose diagrams. Original data are available on request.

RESULTS

New geological site data

The bed investigated by Eriksson & Simpson (2000) is part of one of the largest stream-polished plates in the stream bed, *ca* 1000 m above the base of the Moodies Group (approximate centre of outcrop at 25°42′0.91″S, 31°9′54.08″E; Figs 2 and 3), and is a *ca* 25 m by 25 m large, inclined, perfectly exposed exposure of sandstone on the western bank of Fig Tree Creek (Fig. 3). In this outcrop, 19 beds approximately 0.5 to 3.0 m thick were recognized (Figs 6 and 7).

All units of this outcrop are cross-cut nearly perpendicular to strike by six north–south-trending, minor brittle fault zones *ca* 5 to 40 cm wide with right-lateral and left-lateral offsets of a few centimetres (Figs 5E, 7 and 11). Their style, orientation and quartz-fill show that they are late tectonic features. These structures and accompanying densely-spaced linear and sub-parallel fracture zones are part of a minor fault zone which can be traced intermittently along outcrops along Fig Tree Creek valley, cross-cutting the regional quartzose ridges of Moodies Group sandstones at approximately right angle

and facilitating the incision of the Fig Tree Creek drainage (Figs 2 and 3B).

Facies

The analysis of textural parameters, sedimentary structures and palaeocurrent patterns allows four facies to be recognized (Figs 6 and 8):

1 Facies I consists of thin-bedded sandstone with dominant planar stratification and horizontal lamination, sparsely interbedded with thin laminated siltstone and shale (units D, E, H, K, N and P). Ripples are generally small. Some beds show wispy shale lamination and in places dark grey to black, angular, thin mudchips. Beds of facies I are commonly eroded by beds of Facies IV or Facies III.

2 Facies II consists of thin-bedded to medium-bedded sandstone with abundant and commonly (in two dimensions) bidirectional ripple-drift cross-lamination (units A, C, G, I, L, Q and S). Foreset height is generally small and reaches 5 to 7 cm. Some beds are moderately erosive; they heave out after 1 to 2 m along strike. The mean preserved dune height of *ca* 20 cm suggests approximately 2 m water depth, following the empirical equation of Allen (1984).

3 Facies III is characterized by the presence of contorted bedding, recumbent slump folds in shaly intervals, wispy shale fragments and angular mud chips in medium-bedded sandstone, indicative of nearby occasional subaerial exposure (units O and R). Ripples are rare and poorly developed.

4 Facies IV consists of thick-bedded (up to 1.1 m), moderately erosive sandstone. The beds are internally structured by planar and tangential foresets which may reach up to 1 m thick (units J and M) or by stacked and lenticular cross-bedded sandstone (units B and F). The internal structure of unit J and its origin(s) are analyzed in detail below.

Restored paleocurrents in all units are dominantly directed north-west, with a subordinate current direction, developed in nearly all units, towards the south-east (Fig. 6). Current directions in the channelized sandstone of Facies IV (units B, F, J and M) do not differ substantially from those in the non-channelized Facies II (units A, C, G, I, L, Q and S) and do not vary in orientation significantly with bedform thickness. In unit J, the north-westward direction of transport does not differ substantially between measurements taken in the topset, foreset and bottomset.

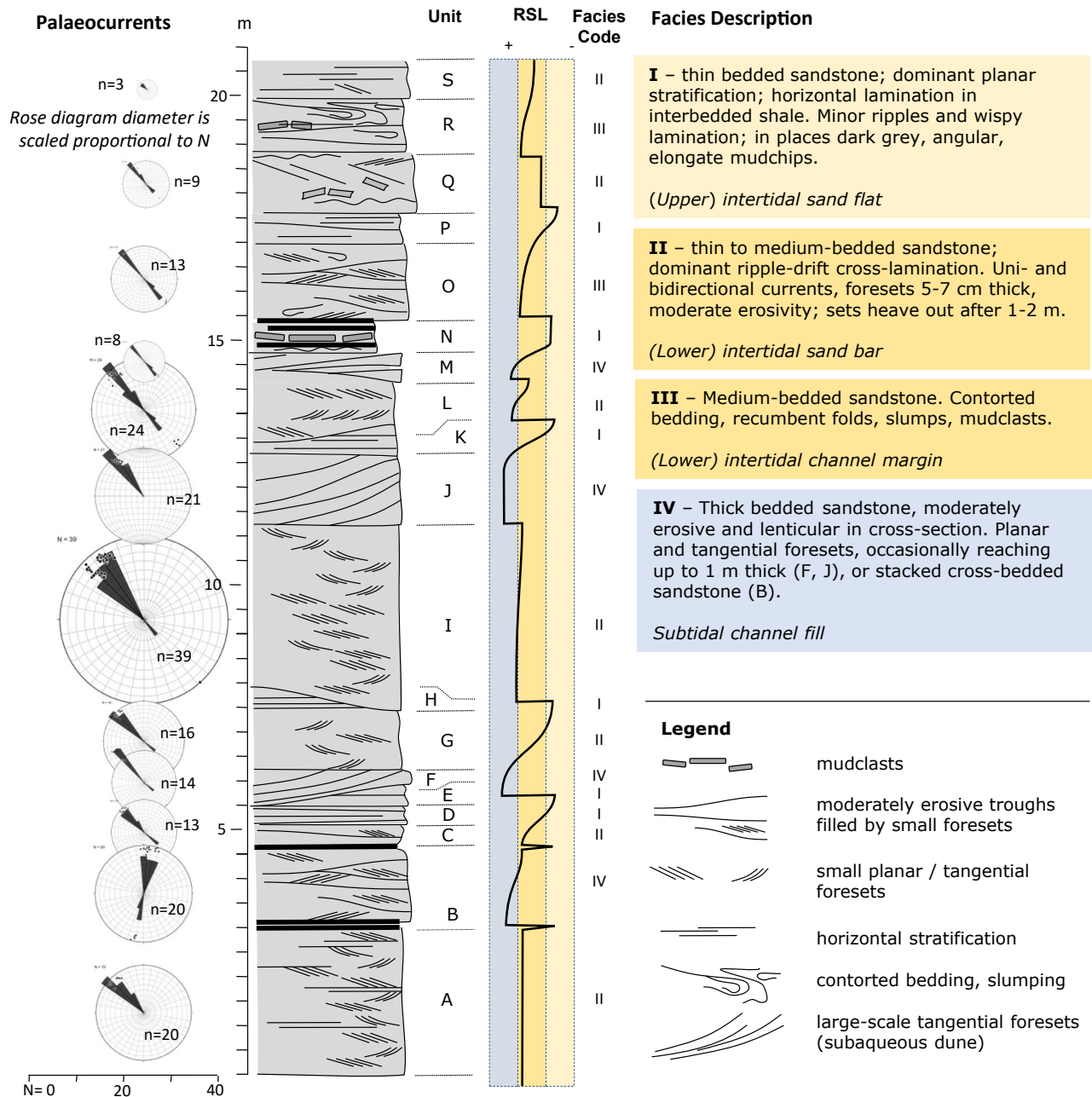


Fig. 6. Stratigraphic column of units exposed on the stream-polished plate in lower Fig Tree Creek. Strata represent lowermost intertidal to subtidal environments in a large mesotidal estuary. The prominent sand wave, focus of this investigation, is unit J. Diameter of polar diagrams is scaled proportionally to the number of measurements. RSL, relative sea level.

Thickness analysis of newly acquired foreset bundles in unit J

Unit J consists of a single bed of quartz-cemented and sericite-cemented sandstone of medium-grained, well-sorted grains of *ca* 0.75 to 1.0 m true stratigraphic thickness (Figs 4 and 5).

Base and top are slightly erosional. The bed is internally structured by a single large foreset of apparent westward progradation (north-westward after correction for plunge and dip) which includes gently inclined topset, moderately inclined foreset and gently inclined toe-sets. Individual bundles are a few millimetres to

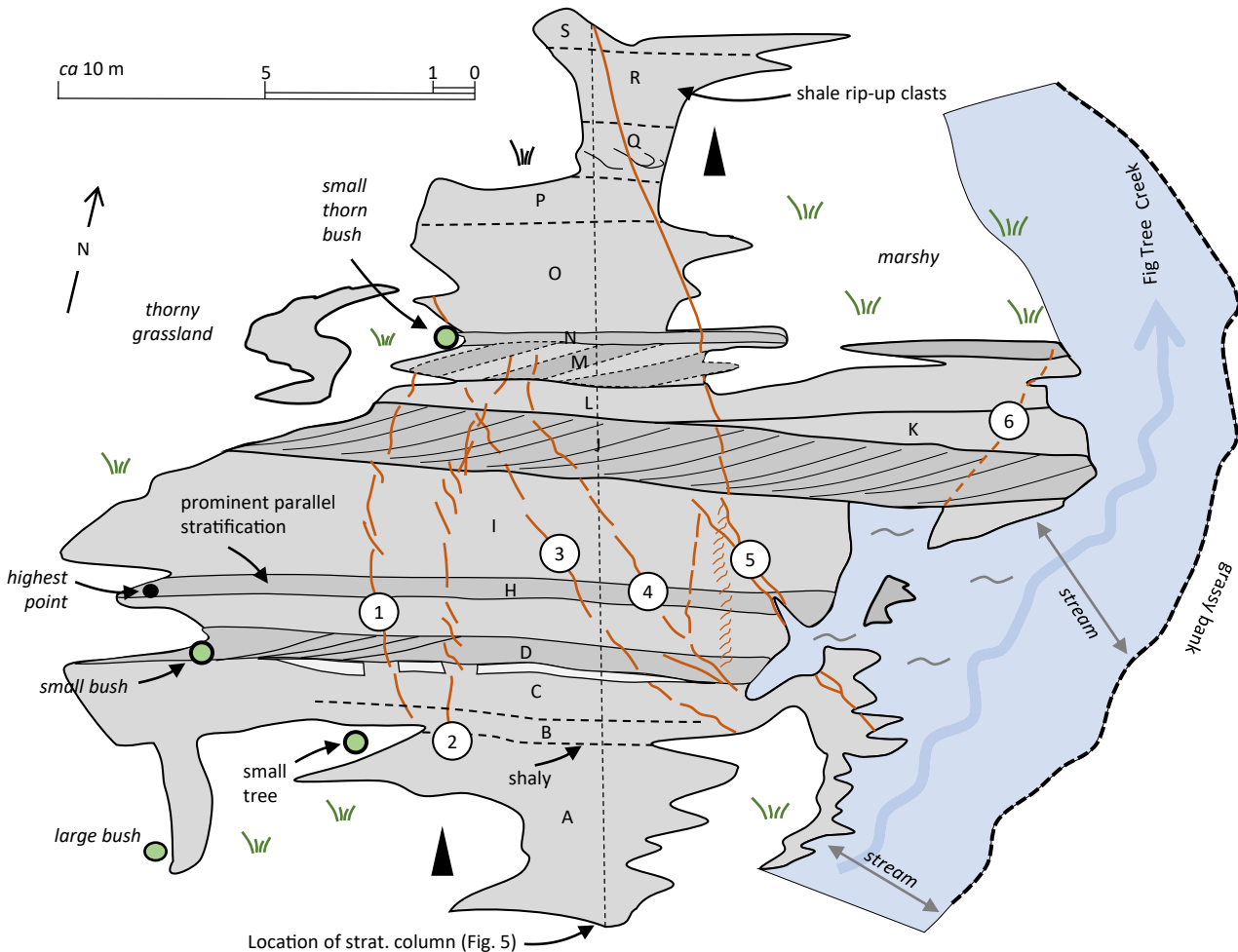


Fig. 7. Geological sketch map of the stream-polished plate in lower Fig Tree Creek. Capital letters denote stratigraphic units shown in Fig. 6, numbered circles indicate fault zones shown in Figs 5E and 11.

ca 30 mm thick; they increase rapidly in thickness near the topset–foreset transition of maximum curvature, maintain a nearly constant thickness over the reach of the foreset, and wedge out gently and with slightly erosional bases in the bottomset. The maximum angle of repose is 23° ; the mean angle of measured foreset inclinations ($n = 21$) after correction for fold plunge and bedding plane dip is 17° (cp. Figs 5C and 6). Sandstone thin section petrography, showing low to moderate compaction, and the excellent preservation of fluid-escape structures in the Fig Tree Creek section suggests that distorting effects of compaction are minor.

Our three repeated measurements of Traverse 2 of Eriksson & Simpson (2000) yielded data sets comprising 62 couplets over 743 mm thickness on the dry rock face in 2014, 68 couplets over 723 mm on the wet rock face in the same year,

and 60 couplets over 737 mm on a dry rock face in 2021 (Fig. 9).

Eriksson & Simpson (2000) recognize a substantially larger number of bundles (118) over approximately the same section length of 743 mm (Fig. 9). The differences in number and thickness of recorded laminae are unlikely to be due to differing locations of the measured sections because all four traverses lie within a few centimetres of one another and laminae do not laterally change thickness significantly over several tens of centimetres or more. The differences in the four data sets from this traverse, including the data of Eriksson & Simpson (2000), may therefore be due to changed exposure, weather, illumination, or, as discussed below, operator bias. Nevertheless, measurements along this traverse appear broadly comparable; that is, bundles of thicker and thinner sandstone–shale

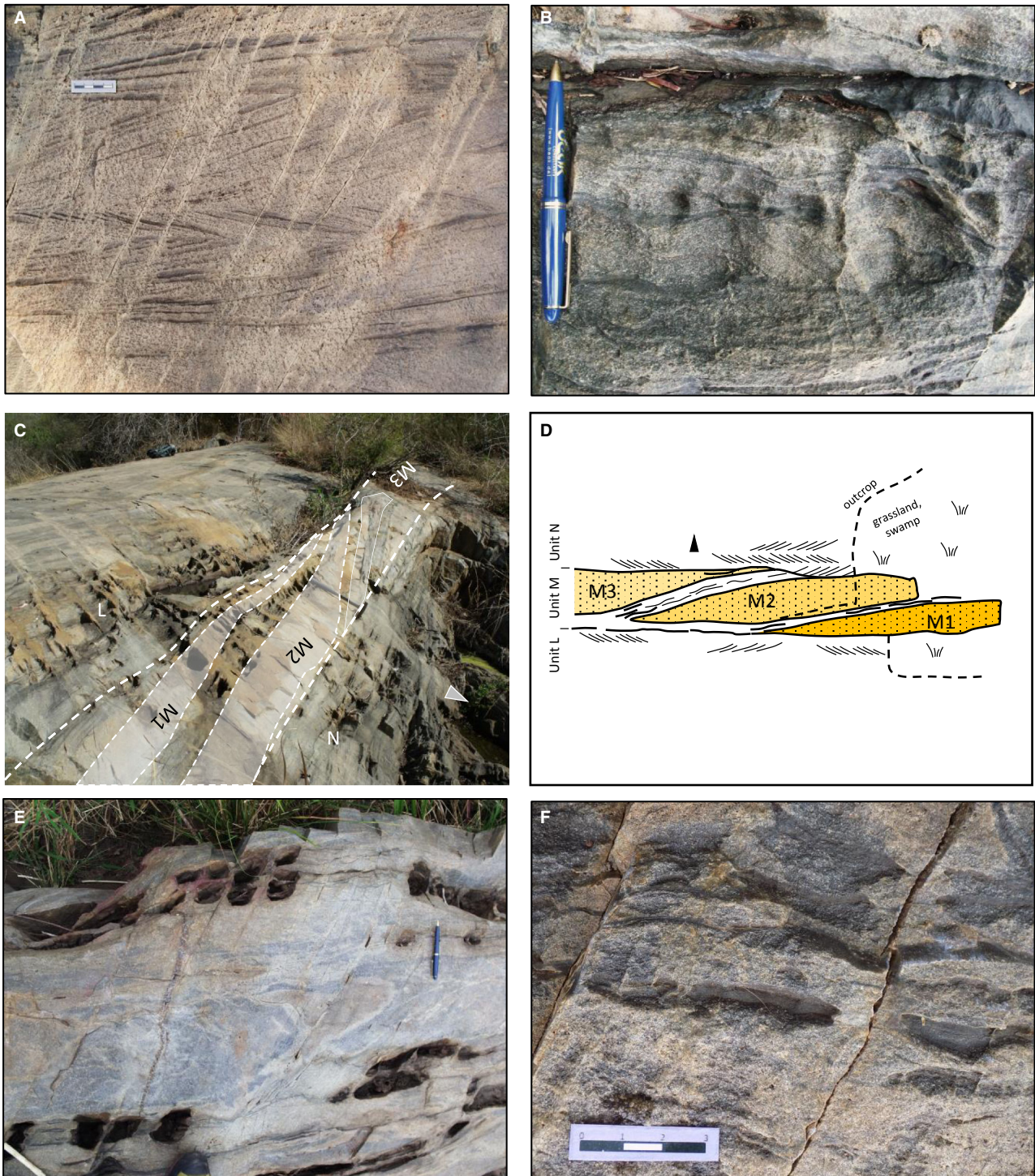


Fig. 8. Sedimentary structures in outcrop. (A) Bidirectional cross-beds, unit I; scale bar is 4 cm long. (B) Angular and wispy mud chips, unit N; pen is 14 cm long. (C) and (D) Laterally migrating sand bars M1 to M3, separated by fine-grained sandstone, unit M; overall thickness of unit M is *ca* 1.1 m. (E) Slump structures in sandstone, unit R; pen is 14 cm long. (F) Wispy shale clasts in sandstone overlying contorted shaly sandstone, unit N; scale is 3 cm long.

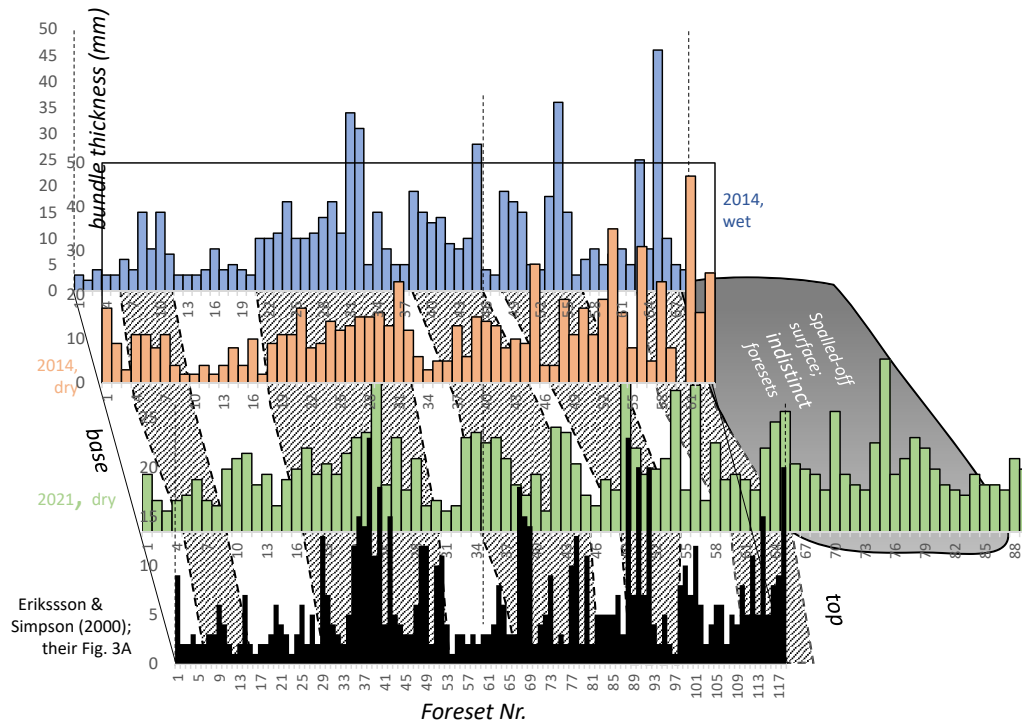


Fig. 9. Comparison of recent measurements (coloured; background) to those of Eriksson & Simpson (2000, fig. 3, foreground). Eriksson & Simpson (2000) recognize significantly more couplets ($n = 118$) compared to the measurements herein ($n = 62, 69$ and 89). Thickness clusters lie, however, at approximately similar positions (grey cross-hatched bands; cp. Fig. 4A).

couplets appear to occur at approximately similar positions within the measured sections (Fig. 7; grey cross-hatched areas in Fig. 9).

Our two additional measurements parallel to bedding between the uphill termination of the outcrop and Fig Tree Creek almost tripled the number of bundles recorded by Eriksson & Simpson (2000; 118 bundles) and yielded data sets of $n = 337$ and $n = 273$ (Fig. 10E and F); however, the traverses had to cross stratigraphic disruptions by Fault Zones 1 to 6, deal with subtly changing outcrop condition towards Fig Tree Creek, and bridge spalled-off slabs which reduce the distinctiveness of laminae (Figs 11 and 12). Measurement teams approached these challenges by tracing laminae along millimetre-offsets across the fault zones.

Finally, a (significantly expanded) composite data set was measured consisting of the remeasured original Traverse 2 of Eriksson & Simpson (2000), enlarged by three correlative sections along strike of the bed (DJvR_CH; Figs 10G and 13). This yielded a data set of 224 bundle thicknesses suitable for time-series analysis.

Figure 14 displays the amplitude spectra of all data sets with and without zero-padding (zero-padding enhances frequency sampling, resulting in higher accuracy in the estimation of the position of the peaks; the frequency resolution, i.e. the width of peaks, remains unchanged). In the original dataset (Fig. 14A), this study confirmed peaks at periods 10.1 and 13.0 bundles per cycle identified by Eriksson & Simpson (2000, fig. 5a); in the reduced data set of Eriksson & Simpson (2000) (Fig. 14B), their modifications were replicated (their fig. 5b): The amplitude of peaks near period 2 is strongly reduced, the peak formerly at a period of 13.0 shifts to 9.5, and periods of 10.1 and 23.6 are nearly completely removed.

The spectra of our two remeasurements of the same traverse under dry (Fig. 14C) and wet (Fig. 14D) conditions, respectively, yield no significant peaks in periodicity in the region of interest. Amplitudes are somewhat lower and peaks shifted to lower periodicities. The lengths of those two traverses are nearly identical to the length of the original data set (74.3 cm, 74.3 cm and 72.3 cm) but comprise fewer bundles (52%

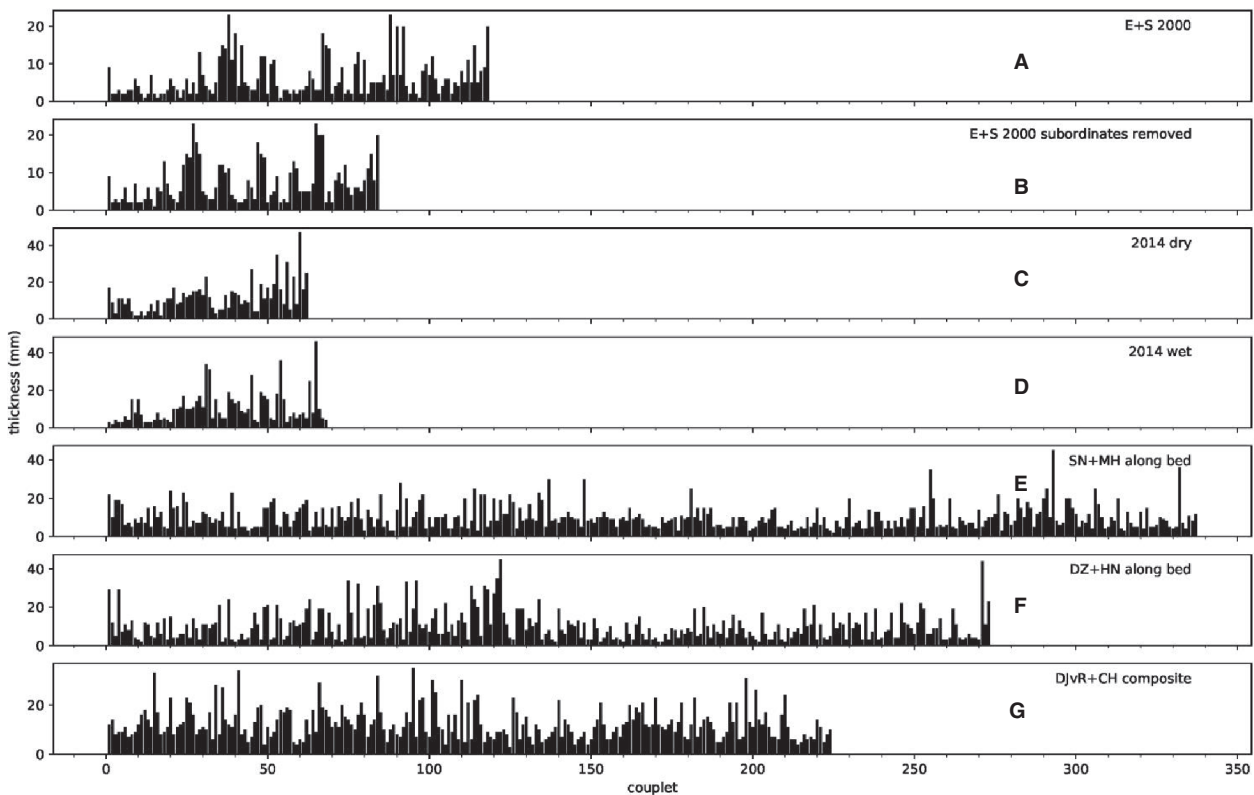


Fig. 10. Histogram of bundle thicknesses with stratigraphic height [(A), (B), (C), (D) and (G)] and along strike [(E) and (F)], respectively. (A), (B), (C) and (D) represent measurements along Traverse 2 of Eriksson & Simpson (2000), measured base-up and oriented perpendicular to bedding. (A) Original data of Eriksson & Simpson (2000). (B) Same data after selectively removing 34 data points (Eriksson & Simpson, 2000). (C) Own measurement of 2014, dry rock face. (D) Same, wet rock face. (E) Measurements parallel to bedding, approximately midway through foresets from uphill end of outcrop (left) to Fig Tree Creek (right), measured by SN and MH. (F) Same, measured by DZ and HN. (G) Composite vertical traverse, shown in detail in Fig. 13.

in Fig. 14C, 57% in Fig. 14D) relative to the 118 data points (100%) in the Eriksson & Simpson (2000) original data set. Our two traverses parallel to bedding and midway in the foreset (Fig. 14E and F) do not show any prominent spectral peaks in the frequency band of interest; they rely on larger data sets than the previous analyses but traverse several fault zones.

The composite data set (Figs 13, 14G and 15) shows distinctive peaks at periods of 14.2 and 9.7, observed similarly in the original data set of Eriksson & Simpson (2000; Fig. 14A). With 224 data points, the data set has a good frequency resolution of 0.0045 cycles per bundle. A harmonic analysis of subsets of this composite data set, each comprising 50 data points offset by 25 data points (Fig. 15), shows the same peak to fluctuate between 12 and 16 with a median at 13.9.

DISCUSSION

Facies

Facies defined at this outcrop (Fig. 6) can be readily interpreted to represent sedimentary processes in a moderate- to high-energy, sand-rich, upper-subtidal estuarine setting which is consistent with the range of depositional interpretations inferred by Eriksson (1977), Eriksson *et al.* (2006) and Heubeck & Lowe (1994a) for the entire Moodies Group.

An (*upper*) *intertidal sand flat* setting combines the sedimentary structures and inferred processes observed in strata of Facies I. Shear stress during sand transport and sedimentation in beds of this facies was apparently high so that bed-forms could not fully develop but intermittent quiet-water conditions allowed mud deposition

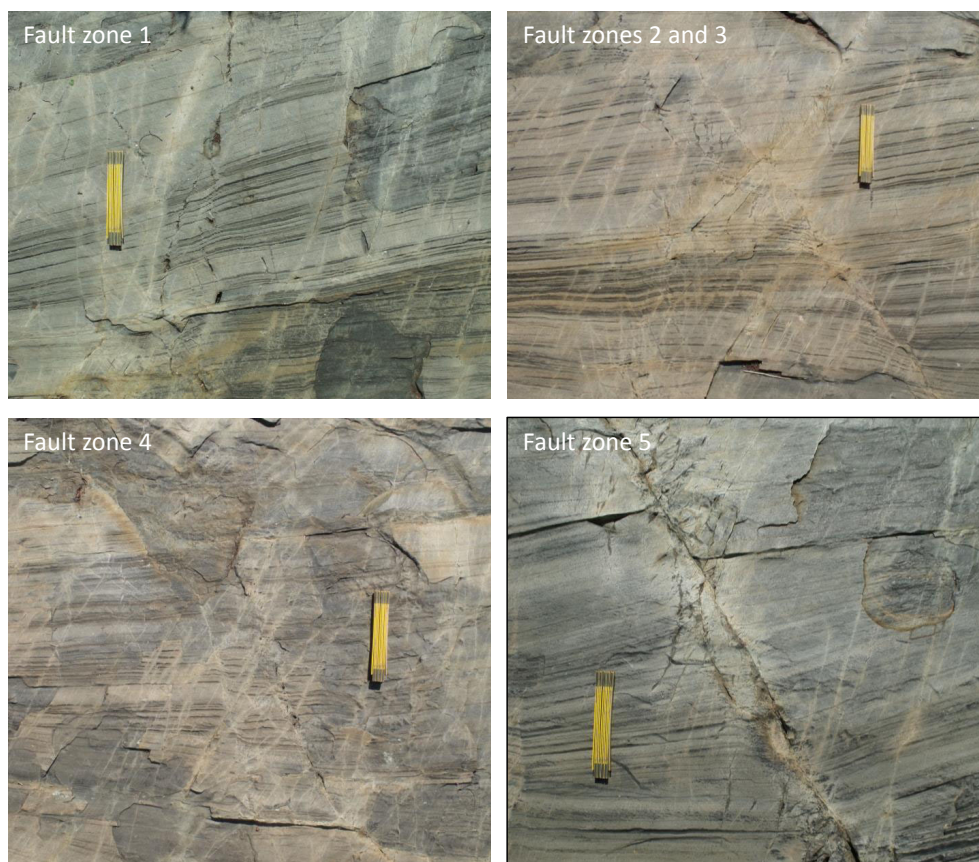


Fig. 11. Map-view photographs of the brittle fracture-and-fault zones transecting unit J shown in Figs 4, 5 and 7; see Fig. 7 for locations. Stratigraphic younging direction is up; scale is 22 cm long. Drag, brittle offset, fracturing, bleaching and spalling of surficially weathered rock plates all combine to render measurements across the fault zones problematic. Scale is 20 cm long.



Fig. 12. Outcrop photographs where slightly weathered, approximately 1 cm thick rock plates in unit J spalled off. Fresh outcrop apparently reduces the bundle contrast. Most-detailed measurements can be made on the lightly weathered rock face. Measurements worked around the spalled-off zones where possible. Pen is 14 cm long.

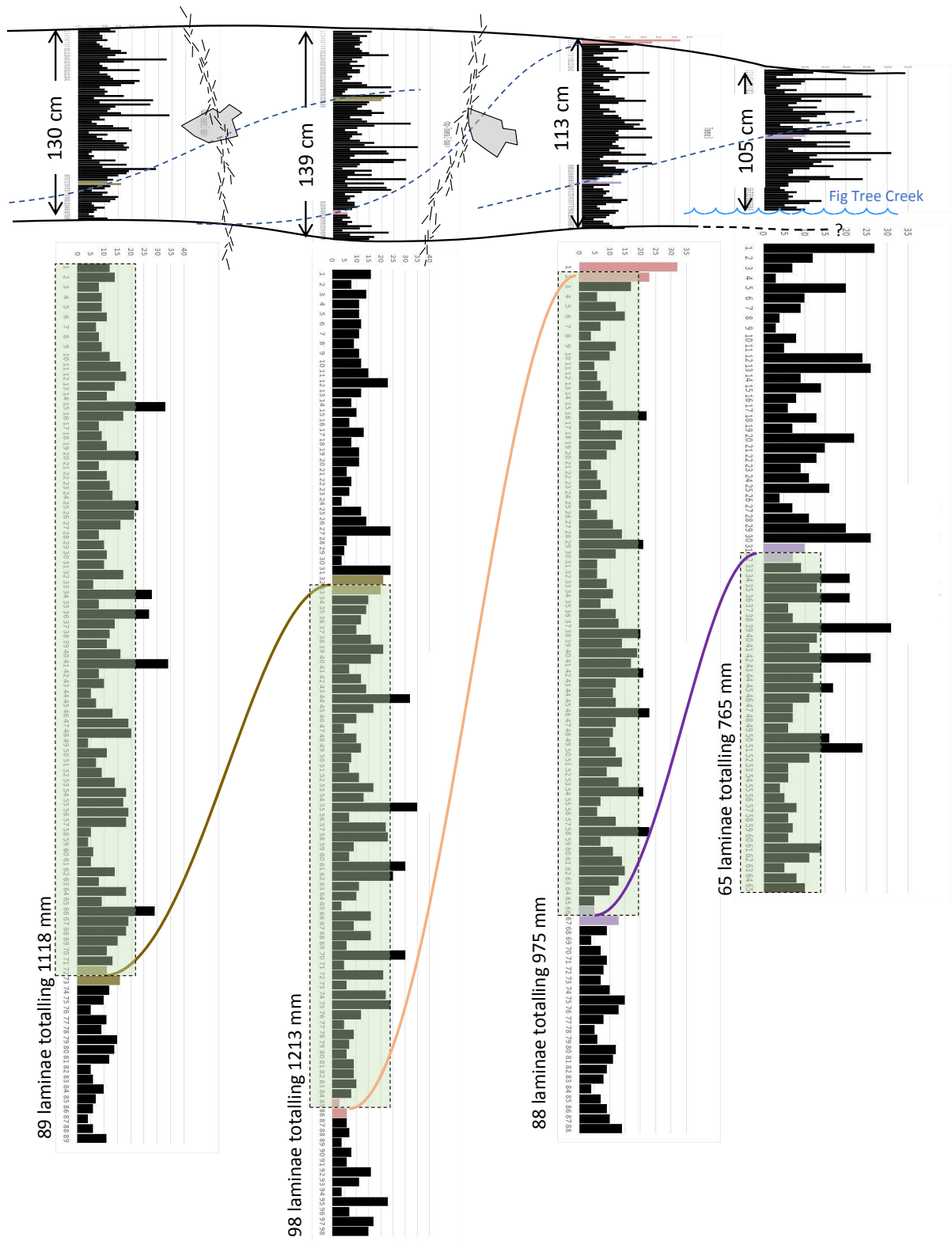


Fig. 13. Extension of the data set of Eriksson & Simpson (2000; leftmost column) by tracing a distinctive foreset lamina near the base of the traverse updip to the top of an adjacent section (*dashed blue line in top diagram*). Total number of laminae ($n = 224$) are marked by light green outline. Histogram bar lengths represent measured laminae thicknesses.

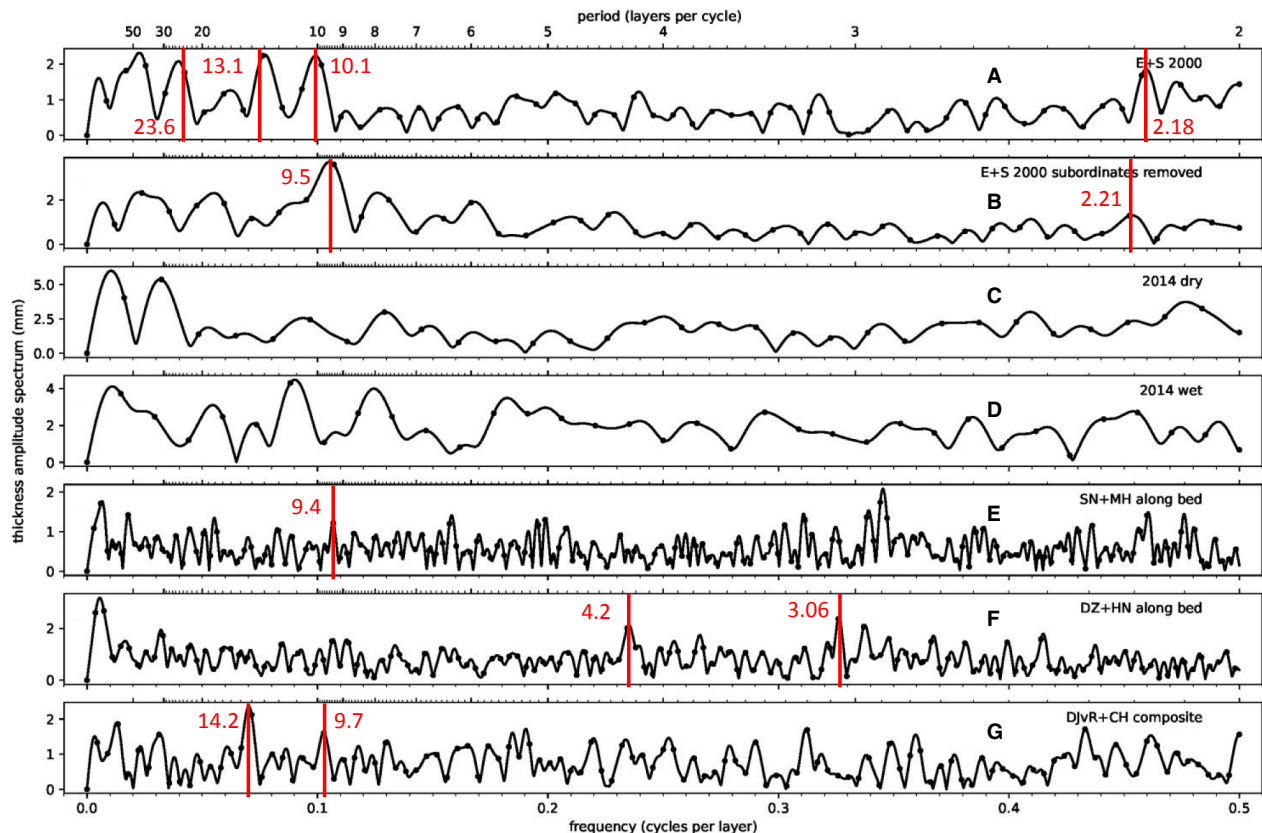


Fig. 14. Harmonic time-series analyses using the fast Fourier transform (FFT) algorithm of bundle thicknesses of unit J shown in Figs 10 and 13. Sources (capital letters) as in Fig. 10. Graph shows Fourier spectra of the original data sets (black dots) and of zero-padded datasets (black lines). Spectra of zero-padded data have the same frequency resolution (i.e. width of peaks) as spectra of unpadded data, but the exact position of peaks can be sampled with higher accuracy. Periodicity peak at 10.1 reported by Eriksson & Simpson (2000, fig. 5A) as 9.833 and 9.33 (their fig. 5B) may be recognizable in data set E (peak at 9.4) and G (peak at 9.7) but other frequencies in data set G, in particular at 14.2, are more pronounced. Period peaks at around 2 in E, F and G are not shown because it can be expected that alternating data points will be of slightly different values.

from suspension. Angular mud chips in unit N (Fig. 8F) demonstrate that mud laminae desiccated during occasional exposure to the atmosphere and were reworked and incorporated in sand beds by storms or by the incoming tide.

(Lower) *intertidal sand bars* typically show sand beds with upper-flow-regime horizontal stratification and abundant bidirectional ripple-drift cross-lamination, observed in Facies II. They indicate dominant strong and reversing currents in or near estuary channels (de Boer *et al.*, 1988; Dalrymple, 1992; Flemming & Bartholomä, 2009).

(Lower) *intertidal channel margins* are characterized by contorted bedding, including recumbent folds (Fig. 8E) in sandstones of units O and R of Facies III. They show that sufficient relief

existed locally to confine flow, detach poorly consolidated strata, and cause lateral slumping (Smith *et al.*, 1991).

Subtidal channel fills have the characteristics observed in Facies IV: Large unidirectional foresets, reflecting grain avalanching by moderately strong currents in several metre water depths, interspersed with thin shale laminae recording slack water and reworking of toesets by counterflow (Klein, 1970; Allen, 1980; Johnson & Baldwin, 1986). The degree of basal erosion by the bases of the channel-fill units F, J and M attests to the strength of the currents. Laterally migrating aggradational sand bars in unit M may represent tidal point bars in curved channels (Roep, 1991; Hughes, 2012; Fig. 8C and D).

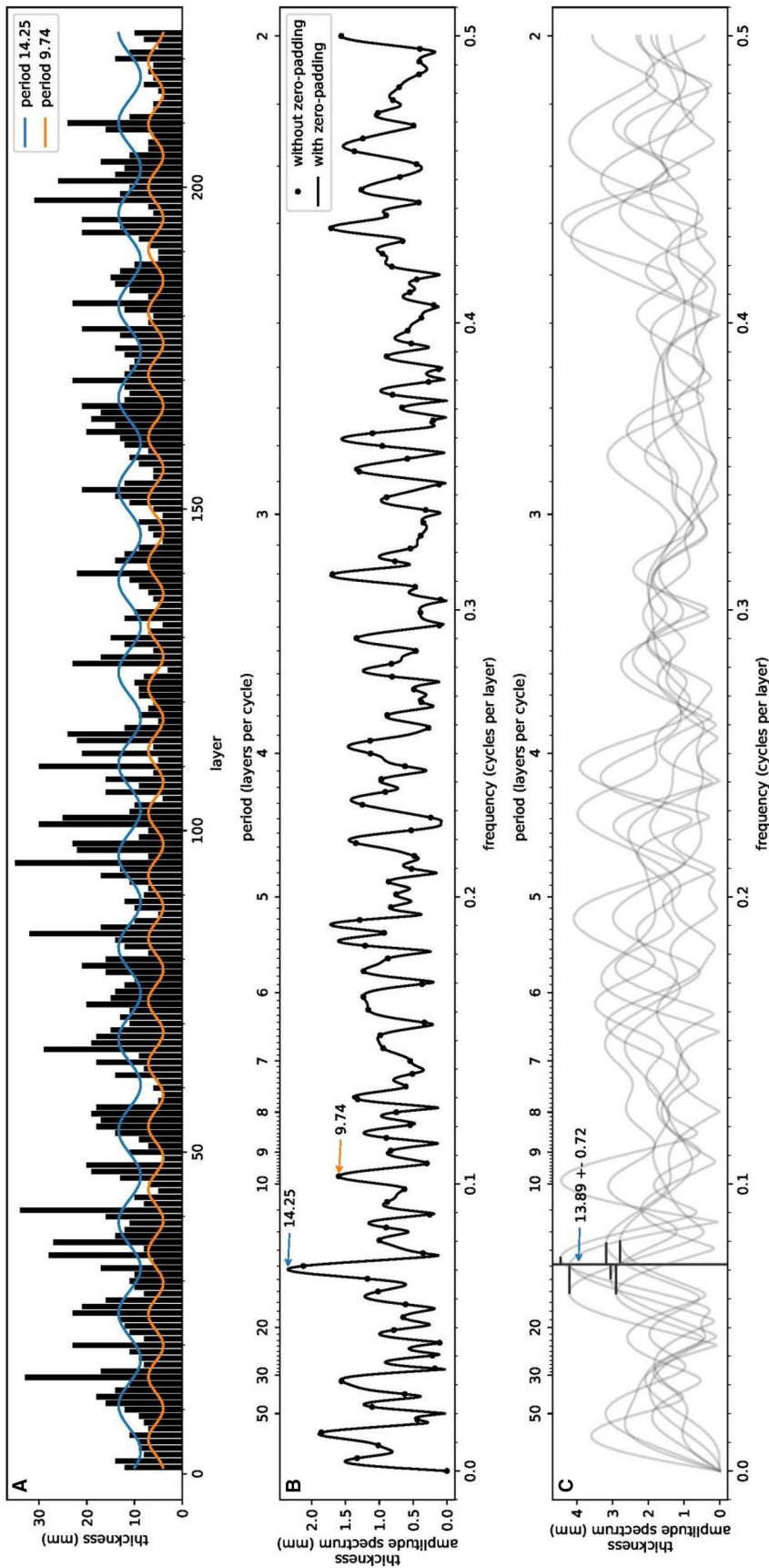


Fig. 15. Time-series analysis of the data set shown in Fig. 13 ($n = 224$), composed of four correlated traverses through the mid-part of the dune foresets. This combination largely avoids the bottomset and topset laminae of uncertain reliability. (A) Histogram of bundle thicknesses superimposed by periodicities recognized in (B) and (C). (B) Amplitude spectrum of this data set (black points) and of the zero-padded data set (continuous line). The frequency bin width and frequency resolution are 0.0045 cycles per bundle for the Fourier transform of the original data set. Frequency sampling is greatly enhanced by zero-padding, contrary to the frequency resolution, which is the same as in the un-padded spectrum. The harmonics corresponding to the two periodicities at 9.74 and 14.25 are displayed in panel (A). (C) Amplitude spectra of seven subsets of the data (grey lines), each comprising 50 data points offset by 25 data points with zero-padding applied. The black vertical line displays the median of the period estimates of the peak of interest for the individual spectra. Residuals are displayed by black horizontal lines. The frequency resolution is mediocre at 0.2 cycles per bundle.

Neither at this site nor elsewhere in the Moodies Group is there evidence of multiple, chaotic superposition of deep-subtidal, intertidal and supratidal sedimentary structures characteristic of hypertidal conditions (Archer, 2013; Heubeck *et al.*, 2016; Heubeck, 2019).

Analysis of unit J

A channel-fill interpretation of unit J is consistent with a medial estuarine environment. This subaquatic dune migrated down-current in a channel similar to but larger than the channel fills of units B, F and M, and, in analogy with those, not more than a few hundred metres distant from intertidal settings where mud chips were periodically produced. Because unit J's preserved thickness of about 1 m includes in places shallowly dipping topsets near the top of the unit and may therefore nearly approach the full bedform height, water depths may have been about 8 m (Allen, 1984), not considering the effects of compaction of perhaps 10%.

Validity of time-series analysis by Eriksson & Simpson (2000)

The systematically varying thicknesses of sandstone–mudstone foreset bundles along a single vertical traverse in unit J were time-series-analyzed by Eriksson & Simpson (2000) (their figs 5A and 5B, replicated in our Fig. 14A and B). Based on the assumption that the original data set represented a semidiurnal tidal pattern (ebb and flood of differing transport capacity approximately twice a day), Eriksson & Simpson (2000) thinned their original data set from 118 to 84 values by removing 34, mostly thin, bundles (Fig. 16). These represent 29% of the bundles and *ca* 16% of the total section thickness, leaving only the record of the dominant daily tide (their fig. 3A and B, replicated in our Fig. 10A and B; see also discussion by Mazumder, 2001, and reply by Eriksson & Simpson, 2001, in which this procedure is defended). This processing inadvertently removed a second major periodicity peak of 13 in the original data set, whose significance will be discussed briefly below. Because the authors assumed that the subordinate tide was inconsistently preserved and the bundle sequence did therefore not represent an even record of time, they did not remove every second sandstone–shale couplet (only 19 of the 34 removed bundle thicknesses are alternating) but in places removed every third, fourth, fifth, etc. bundle (Fig. 16A and B),

leaving sets of 6, 9, 11 and 13 bundles unchanged (Fig. 16B). Removed couplets are often, but not always, subordinate in thickness to adjacent bundles (Fig. 16C).

The selective removal of bundles eliminated periodicity peaks of 24, 13 and 2 (Fig. 14B). The remaining periodicity peak of 9.33 (9.5 in our analysis) was interpreted to highlight a strong lunar semimonthly signature of nine to ten lunar days. From that number, they (incorrectly) inferred the duration of the anomalistic month (that is, perigee to perigee on an elliptical orbit, currently 27 days 13 h) as twice that number, that is, approximately 18 to 20 days. More correctly, the comparison should have been made to the synodic (New Moon to New Moon) month, currently 29 days 13 h.

Eriksson & Simpson (2000) describe probably the best exposure of a quantifiable tidal data set from the Moodies Group and possibly from the Palaeoarchean (>3.2 Ga). Nowhere else, to the knowledge of the authors, exist exposures of a comparable size and quality as in the lower Moodies Group strata in Fig Tree Creek. The authors agree with Eriksson & Simpson's (2000) interpretation of unit J as a large migrating subaqueous sand wave. It also appears plausible that thickness variations of its foresets may be related to variations in the strength of tidal currents. The authors believe, however, that several factors seriously affect Eriksson & Simpson's (2000) data set and invalidate their conclusion of an anomalistic month of 18 to 20 days length.

- *Incompleteness of record:* Unit J occupied the medial to outer part of a major tidal channel, approximately 8 m deep and hundreds of metres wide, which likely formed part of an extensive estuary system of tidal sandflats, channel margins, channels and sand bars comparable to some modern settings (for example, the outer Elbe estuary, Germany, Wever & Stender, 2000; the Jade estuary, Germany, Zeiler *et al.*, 2000; outer Chesapeake Bay, USA, Perillo & Ludwick, 1984). Stratigraphic analysis from other parts of the Moodies Group in comparable lithologies (Heubeck *et al.*, 2016) allows to infer mesotidal conditions. In such a setting, large subaquatic dunes are susceptible to omission of laminae (Klein, 1970; Visser, 1980; Boothroyd, 1985; Yang & Nio, 1985; Williams, 1991) by storms, floods or avulsion of channels. In order to fully record daily or twice-daily tidal information, a sand dune should therefore be located farther offshore where currents are steadier (de Boer

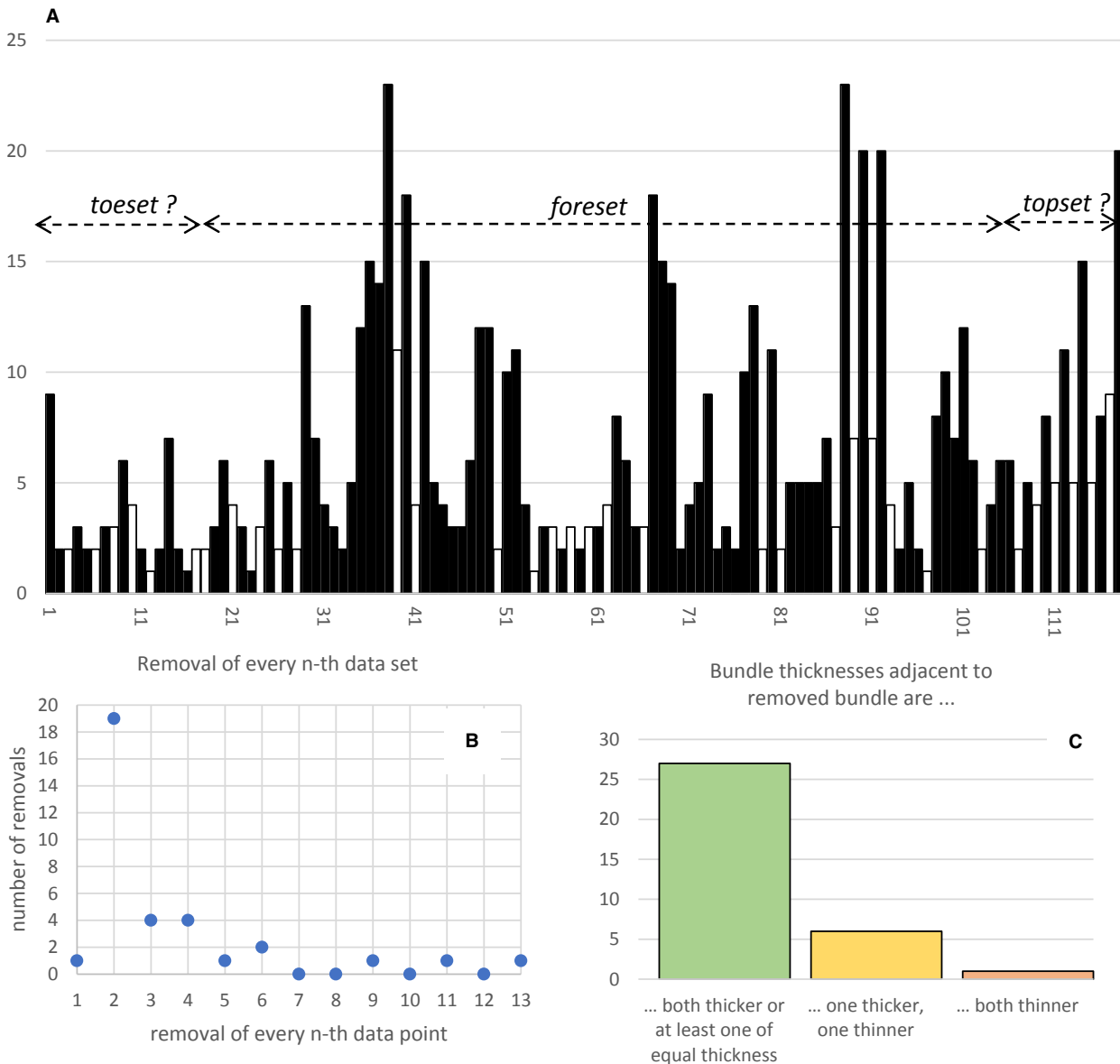


Fig. 16. Analysis of data processing performed by Eriksson & Simpson (2000) to remove: “... inferred subordinate flood-tide sandstone bundles”. (A) Original data set of Eriksson & Simpson (2000) showing (as white bars) the bundles removed by the authors prior to time-series analysis. (B) Only 19 of the 34 data points are alternating (every second data point); the remainder are unevenly distributed. Packages of 5, 6, 9, 11 and 13 adjacent measurements were left unmodified. (C) Removed bundles are mostly but not always the thinnest bundle between thicker bundles.

et al., 1988; Sonett & Chan, 1998; Flemming & Bartholomä, 2009). Although tidal rhythmite data as short as four months can provide suitable estimates of lunar orbital periods if these records are complete (Kvale *et al.*, 1999), non-deposition or erosion of a single laminae within any 14-couplet bundle set would result in inferring a nearer moon orbit, a possibility recognized by Eriksson & Simpson (2000).

Observations by Yang & Nio (1985) suggest that time series of 40 bundles or more may also record the growth and decay of a bedform with consequences for the thickness of foresets, its interference with other bedforms, or the subtle change in its orientation.

While the peak around 14 bundles shows the highest spectral power, its prominence, compared to several other peaks, is not high. This

indicates that the data set is 'noisy'. Bundle thickness series may be partially compromised by complete or partial erosion or truncation of certain beds, or by non-deposition. This 'noisiness' is difficult to quantify.

- *Orientation of traverse:* Eriksson & Simpson's (2000) data set represents a traverse which was measured perpendicular to bedding and therefore begins in basal toesets, traverses main foresets and ends in topsets (assuming that the section was measured from base upward). This orientation has the advantage of avoiding complications by one of the six minor fault zones which cut the exposure of unit J at approximately right angle; however, any such traverse should probably be verified by measuring additional traverses a few metres along strike. Laminae thickness analyses perpendicular to bedding may also be problematic because lee-eddy-generated counterflows and differential avalanche runouts are prone to modify thicknesses of toset laminae (Reineck & Wunderlich, 1968; Allen, 1985; Dalrymple, 1992). All datasets measured perpendicular to bedding (Figs 4 and 9; data sets A, B, C and D of Fig. 10) indeed show anomalously thin basal strata [for example, in the Eriksson & Simpson (2000) data set, couplets 1 to 28; Fig. 16A]. All topset thicknesses, in contrast, are endangered by episodic erosional avalanching and scalloping; the top-most 20 cm of the Eriksson & Simpson (2000) dataset are anomalously thick (couplets 105 to 118; Fig. 16A), as are datasets A, B and C in Fig. 9. Because of the suboptimal orientation of the traverse, the authors consider the conclusions drawn from data sets of this orientation unreliable and ambiguous. Data set G (Fig. 13) avoids many but not all bottomsets and topsets and may thus be more informative.

- *Data processing:* The selective removal of measured data to remove the uneven preservation of a suspected minor semidiurnal tide wave was inconsistently applied, perhaps because Eriksson & Simpson (2000) interpreted the data set to reflect a mixed tidal system which shows both semi-diurnal and diurnal sedimentation. However, although raw data may require refinement to yield equidistant sampling and to make periodicities apparent (e.g. De Boer *et al.*, 1989; Kvale *et al.*, 1999; Coughenour *et al.*, 2009), the data set in question appears to be too short to be amenable for such an analysis (Williams, 2005).

- *Representativeness:* As also recognized by Eriksson & Simpson (2000), it is impossible to know whether the sand wave, the outcrop, the sand-dominated unit MdS1, the Moodies Group or even greenstone belts in general are representative of global tectonic and sedimentary processes (de Wit & Ashwal, 1995; Lowe & Byerly, 1999). Even today, most tidal strata are dominated not by the Moon–Earth orbital dynamics but rather by local, regional or ocean basin parameters, such as basin geometry, seasonal variations in fluvial discharge, or climate. From an analysis of randomly selected Recent tidal strata, one would probably not be able to conclude that Earth was circled by a single moon in an elliptical orbit in 28 days (Roep, 1991; Cowan *et al.*, 1998).

- *Reproducibility and operator bias:* Fresh exposures, where slightly weathered rinds had spalled off, showed markedly indistinct laminae compared to surrounding patterns on slightly weathered rock faces (Fig. 12). Thin coatings by dust, microbial films, wetness, daytime-varying exposure to intensity and direction of sunlight, resulted in significant variations in our repeated measurements. In addition, it was found that operator bias (individuals observing the same data under identical conditions would make different observations) has the potential to systematically affect periodicities: 'Splitters' will generate lower-frequency, 'lumpers' higher-frequency data sets.

Earth–Moon dynamics

The dynamics of the Earth–Moon system are governed by the conservation of angular momentum and its transfer from the Earth's rotation to the Moon's orbital motion by tidal friction. This requires that the length of day (duration of time from sunrise to sunrise, measuring the spin rate of the Earth), the length of lunar synodic months (time from Full Moon to Full Moon) and the Earth–Moon distance are quantitatively related. As Earth's rotation slows down and days become longer, the Moon moves into a higher elliptical orbit with a longer period. This relationship is readily quantified by equations of orbital mechanics considering conservation of angular momentum (Runcorn, 1979; Webb, 1982; Williams, 2000; Williams, 2005; Meyers & Malinverno, 2018; Tyler, 2021). The largely successful removal of periodicities of two (every other data set is of a significantly different thickness) by Eriksson & Simpson (2000) also

removed the most dominant peak of their data set, a periodicity of 13.11 (their fig. 5A and B), leaving them with a dominant spectral peak of nine or ten. They interpreted this peak as the number of diurnal tides from spring tide (Full Moon) to neap tide (Half Moon) to spring tide (New Moon); doubling this time interval yielded a synodic month (Full Moon to Full Moon) approximately 18 to 20 days long, compared to a present-day value of 29.5.

The authors see no reason, however, to remove the prominent 13.11 spectral peak and also observe a similar peak of 14.2 in one of our best data sets (Fig. 15). If real, a frequency of 13 to 14 would indicate approximately 26 to 28 lunar days per synodic month, similar to today's value of 29.5, or to the 27.6 days of the anomalistic month. The data sets examined here, although clearly far from ideal, must thus be interpreted in the context of a closer, faster-orbiting Archean Moon circling a faster-spinning Archean Earth.

CONCLUSIONS

It would be highly desirable to have robust early-Earth data constraining the Moon–Earth system. Because of its old age, widespread tidal-facies strata, low degree of deformation, and occasional good exposure, the Moodies Group of the Barberton Greenstone Belt is a well-suited unit to provide such data, and the subaquatic sand dune investigated by Eriksson & Simpson (2000) likely constitutes the best outcrop amenable to such an analysis. It comprises to date the only Archean data point. Sandstone–shale bundles show abundant rhythmic bedding and may contain tidal information; however, outcrop facies analysis suggests that the depositional setting was probably located too close to supratidal and high-energy shorelines to reliably record months-long tidal signals; individual laminae may have been non-deposited or removed by erosion. In addition, this study cannot fully reproduce Eriksson & Simpson's (2000) data set, considers the orientation of their measured traverse suboptimal, and finds their data-processing approach problematic.

The repeated measurements of the foresets herein followed three strategies but only a composite data set of several correlated mid-foreset traverses recorded a robust periodicity peak at approximately 14 bundles per cycle, a peak observed with a similar value (but then eliminated) by Eriksson & Simpson (2000). The authors interpret this approximately 28-lunar-

days-per-synodic-month periodicity as representing a state during which a closer, faster-orbiting Archean Moon circled a faster-spinning Archean Earth. The consequences for other orbital parameters will be investigated in a separate study.

Scientific drilling in the Moodies Group of the Barberton Greenstone Belt through fine-grained subtidal and prodelta strata may yield longer and more continuous records through unweathered rocks. These may contribute to constrain Moon–Earth dynamics more reliably from the Archean sedimentary record than other data sources.

ACKNOWLEDGEMENTS

Field work was begun while some of the authors were students or employed at the FU Berlin, Institut für Geologische Wissenschaften, and partially supported by DAAD scholarships. C. Heubeck, M. Homann and S. Nabhan were supported by DFG grants He2418/13-1, 14-1 and 22-1. Chris Rippon provided initial information on outcrop location. The people of Barberton, in particular Astrid Christianson, Adriaan and Lili Nel, and Tony and Sandy Ferrar were, as ever, gracious hosts. Duwies Duvenage of Barberton Toyota is thanked for providing mobility in the field. Comments by Ed Simpson and Rajat Mazumder improved an early version of the manuscript. We thank two anonymous reviewers for detailed and thorough comments. Open Access funding enabled and organized by Projekt DEAL.

CONFLICT OF INTEREST

We declare that we have no commercial or associative aim that might represent a conflict of interest in connection with the work submitted.

DATA AVAILABILITY STATEMENT

The data that support the findings of this study are available from the corresponding author upon reasonable request.

REFERENCES

- Allen, J.R.L. (1980) Sand waves: a model of origin and internal structure. *Sediment. Geol.*, **26**, 281–326.
- Allen, J.R.L. (1982) Mud drapes in sand-wave deposits: a physical model with application to the Folkestone Beds

- (Early Cretaceous, southeast England). *Philos. Trans. R. Soc. Lond. Ser. A*, **306**, 291–345.
- Allen, J.R.L.** (1984) *Sedimentary Structures: Their Character and Physical Basis, Developments in Sedimentology*, 30. Elsevier, Amsterdam, 1256 pp.
- Allen, J.R.L.** (1985) *Principles of Physical Sedimentology*. George Allen & Unwin, London, 272 pp.
- Allmendinger, R.W., Cardozo, N. and Fisher, D.** (2011) *Structural Geology Algorithms: Vectors and Tensors in Structural Geology*. Cambridge University Press, Cambridge, 302 pp.
- Anhaeusser, C.R.** (1976) The geology of the Sheba Hills area of the Barberton Mountain Land, South Africa, with particular reference to the Eureka Syncline. *South Afr. J. Geol.*, **79**, 253–280.
- Archer, A.** (1996) Reliability of lunar orbital periods extracted from ancient cyclic tidal rhythmites. *Earth Planet. Sci. Lett.*, **141**, 1–10.
- Archer, A.** (2013) World's highest tides: hypertidal coastal systems in North America, South America and Europe. *Sed. Geol.*, **284–285**, 1–25.
- Bills, B.G. and Ray, R.D.** (1999) Lunar orbital evolution: a synthesis of recent results. *Geophys. Res. Lett.*, **26**, 3045–3048.
- Boothroyd, J.C.** (1985) Tidal inlets and tidal deltas. In: *Coastal Sedimentary Environments* (Ed. Davis, R.A.), pp. 445–532. Springer-Verlag, New York.
- Brosche, P.** (1984) Tidal friction in the Earth-Moon system. *Philos. Trans. R. Soc. Lond. Ser. A*, **313**, 71–75.
- Byerly, G.R., Lowe, D.R. and Heubeck, C.** (2018) Geologic evolution of the Barberton Greenstone Belt – a unique record of crustal development, surface processes, and early life 3.55 to 3.20 Ga. In: *Earth's Oldest Rocks – Second Edition* (Eds Van Kranendonk, M.J., Bennett, V.C. and Hoffmann, J.E.), pp. 569–613. Elsevier, Amsterdam.
- Cardozo, N. and Allmendinger, R.W.** (2013) Spherical projections with OSXStereonet. *Comput. Geosci.*, **51**, 193–205.
- Chan, M.A., Kvale, E.P., Archer, A.W. and Sonett, C.P.** (1994) Oldest direct evidence of lunar-solar tidal forcing in sedimentary rhythmites, proterozoic big cottonwood formation, central Utah. *Geology*, **22**, 791–794.
- Coughenour, C.L., Archer, A.W. and Lacovara, K.J.** (2009) Tides, tidalites, and secular changes in the Earth-Moon system. *Earth Sci. Rev.*, **97**, 59–79.
- Cowan, E.A., Cai, J., Powell, R.D., Seramur, K.C. and Spurgeon, V.L.** (1998) Modern tidal rhythmites deposited in a deep-water estuary. *Geo-Mar. Lett.*, **18**, 40–48.
- Dalrymple, R.W.** (1992) Tidal depositional systems. In: *Facies Models: Response to Sea Level Changes* (Eds Walker, R.G. and James, N.P.), pp. 195–218. Geological Association of Canada, Newfoundland, Canada.
- De Boer, P.L., van Gelder, A. and Nio, S.D.** (Eds). (1988) *Tide-Influenced Sedimentary Environments and Facies*. Kluwer Academic Publishers, Amsterdam.
- De Boer, P.L., Oost, A.P. and Visser, M.J.** (1989) The diurnal inequality of the tide as a parameter for recognizing tidal influences. *J. Sediment. Petrol.*, **59**, 912–921.
- Dickey, J.O., Bender, P.L., Faller, J.E., Newhall, X.X., Ricklefs, R.L., Ries, J.G., Shelus, P.J., Veillet, C., Whipple, A.L., Wiant, J.R., Williams, J.G. and Yoder, C.F.** (1994) Lunar laser ranging: a continuing legacy of the Apollo program. *Science*, **265**, 482–490.
- Eriksson, K.A.** (1977) Tidal flat and subtidal sedimentation in the Malmani Dolomite, South Africa. *Sed. Geol.*, **18**, 223–244.
- Eriksson, K.A.** (1979) Marginal marine depositional processes from the Archaean Moodies Group, Barberton Mountain Land, South Africa: evidence and significance. *Precambrian Res.*, **8**, 153–182.
- Eriksson, K.A. and Simpson, E.L.** (2000) Quantifying the oldest tidal record: the 3.2 Ga Moodies Group, Barberton Greenstone Belt, South Africa. *Geology*, **28**, 831–834.
- Eriksson, K.A. and Simpson, E.L.** (2001) Reply to: Quantifying the oldest tidal record: the 3.2 Ga Moodies Group, Barberton Greenstone Belt, South Africa. *Geology*, **29**, 1159–1160.
- Eriksson, K.A., Simpson, E.L. and Mueller, W.** (2006) An unusual fluvial to tidal transition in the meso-Archaean Moodies Group, South Africa: a response to high tidal range and active tectonics. *Sed. Geol.*, **190**, 13–24.
- Eriksson, P.G., Banerjee, S., Catuneanu, O., Corcoran, P., Eriksson, K.A., Hiatt, E.E., Laflamme, M., Lenhardt, N., Long, D.G.F., Miall, A., Mints, M.V., Pufahl, P.K., Sarkar, S., Simpson, E.L. and Williams, G.E.** (2013) Secular changes in sedimentation systems and sequence stratigraphy. *Gondwana Res.*, **24**, 468–489.
- Flemming, B.W. and Bartholomä, A.** (Eds). (2009) *Tidal Signatures in Modern and Ancient Sediments*. Blackwell Science, Oxford, 368 pp.
- Friedman, G.M. and Chakraborty, C.** (2006) Interpretation of tidal bundles: two reasons for a paradigm shift. *Carbonates Evaporites*, **21**, 170–175.
- Friedman, G.M., Sanders, J.E. and Kopaska-Merkel, D.C.** (1992) *Principles of Sedimentary Deposits: Stratigraphy and Sedimentology*. Macmillan Publishing Company, New York, 717 pp.
- Green, J.A.M., Huber, M., Waltham, D., Buzan, J. and Wells, M.** (2017) Explicitly modelled deep-time tidal dissipation and its implication for Lunar history. *Earth Planet. Sci. Lett.*, **461**, 46–53.
- Hansen, K.S.** (1982) Secular effects of oceanic tidal dissipation on the Moon's orbit and the Earth's rotation. *Rev. Geophys. Space Phys.*, **20**, 457–480.
- Hessler, A.M. and Lowe, D.R.** (2006) Weathering and sediment generation in the Archaean: an integrated study of the evolution of siliciclastic sedimentary rocks of the 3.2 Ga Moodies Group, Barberton Greenstone Belt, South Africa. *Precambrian Res.*, **151**, 185–210.
- Heubeck, C.** (2019) The Moodies Group – a high-resolution archive of Archaean surface and basin-forming processes. In: *The Archaean Geology of the Kaapvaal Craton, Southern Africa* (Eds Kröner, A. and Hofmann, A.), pp. 203–241. Springer (Regional Geology Reviews), Cham, Switzerland.
- Heubeck, C., Bläsing, S., Drabon, N., Grund, M., Homann, M. and Nabhan, S.** (2016) Geological constraints on Archean (3.22 Ga) coastal-zone processes from the Dycedale Syncline, Barberton Greenstone Belt. *South Afr. J. Geol.*, **119**, 495–518.
- Heubeck, C., Drabon, N., Byerly, G., Leisgang, I., Linnemann, U., Lowe, D.R., Merz, R., Gonzalez-Pinzon, A., Thomsen, T., Zeh, A., Rojas Agramonte, Y. and Kröner, A.** (2022) Constraints by detrital zircons on the provenance of the Archean Moodies Group, Barberton Greenstone Belt, South Africa and Eswatini. *Am. J. Sci.*, in press.
- Heubeck, C., Engelhardt, J., Byerly, G.R., Zeh, A., Sell, B., Lubert, T. and Lowe, D.R.** (2013) Timing of deposition and deformation of the Moodies Group (Barberton Greenstone Belt, South Africa): very-high-resolution of Archaean surface processes. *Precamb. Res.*, **231**, 236–262.

- Heubeck, C. and Lowe, D.R. (1994a) Depositional and tectonic setting of the Archean Moodies Group, Barberton Greenstone Belt, South Africa. *Precambrian Res.*, **68**, 257–290.
- Heubeck, C. and Lowe, D.R. (1994b) Late syndepositional deformation and detachment tectonics in the Barberton Greenstone Belt, South Africa. *Tectonics*, **13**, 1514–1536.
- Heubeck, C. and Lowe, D.R. (1999) Sedimentary petrology and provenance of the Archean Moodies Group, Barberton Greenstone Belt, South Africa. In: *Geologic Evolution of the Barberton Greenstone Belt, South Africa* (Eds Lowe, D.R. and Byerly, G.R.), Geological Society of America Special Paper 329, pp. 259–286. Geological Society of America, Boulder, CO.
- Homann, M., Heubeck, C., Airo, A. and Tice, M.M. (2015) Morphological adaptations of 3.22 Ga-old tufted microbial mats to Archean coastal habitats (Moodies Group, Barberton Greenstone Belt, South Africa). *Precambrian Res.*, **266**, 47–64.
- Hughes, Z.J. (2012) Tidal channels on Tidal flats and marshes. In: *Principles of Tidal Sedimentology* (Eds Davis R.A. and Dalrymple, R.W.), pp. 269–300. Springer, Dordrecht.
- Johnson, H.D. and Baldwin, C.T. (1986) Shallow siliciclastic seas. In: *Sedimentary Environments and Facies* (Ed. Reading, H.G.), pp. 229–282. Blackwell, Oxford.
- Kagan, B.A. (1997) Earth–Moon tidal evolution: model results and observational evidence. *Prog. Oceanogr.*, **40**, 109–124.
- Kagan, B.A. and Sündermann, J. (1996) Dissipation of tidal energy, paleotides, and evolution of the Earth–Moon system. *Adv. Geophys.*, **38**, 179–266.
- Kessler II, L.G. and Gollop, I.G. (1988) Inner shelf/shoreface–intertidal transition, upper Precambrian, Port Askaig Tillite, Isle of Islay, Argyll, Scotland. Symposium on Clastic Tidal Deposits: Tide-influenced Sedimentary Environments and Facies. D. Reidel Publ. Co., Dordrecht.
- Klein, G.V. (1970) Depositional and dispersal dynamics of intertidal sand bars. *J. Sediment Petrol.*, **40**, 1095–1127.
- Kvale, E. (2006) The origin of neap–spring tidal cycles. *Mar. Geol.*, **235**, 5–18.
- Kvale, E. (1997) Tidal rhythmites and their applications: Indiana Geological Survey, Bloomington, Indiana, Open-File Study 96-06, 104 p.
- Kvale, E.P., Johnson, H.W., Sonett, C.P., Archer, A.W. and Zawistoski, A. (1999) Calculating lunar retreat rates using tidal rhythmites. *J. Sediment. Res.*, **69**, 154–168.
- Lambeck, K. (1980) *The Earth's Variable Rotation: Geophysical Causes and Consequences*. Cambridge Univ. Press, New York.
- Longhitano, S.G., Mellere, D., Steel, R.J. and Ainsworth, R.B. (2012) Tidal depositional systems in the rock record: a review and new insights. *Sed. Geol.*, **279**, 2–22.
- Lopez de Azarevich, V.L. and Azarevich, M.B. (2017) Lunar recession encoded in tidal rhythmites: a selective overview with examples from Argentina. *Geo Mar. Lett.*, **37**, 333–344.
- Lowe, D.R. and Byerly, G.R. (1999) Geological evolution of the Barberton Greenstone Belt, South Africa. *Geol. Soc. Amer., Spec. Pap.*, **329**, 319 p.
- Lowe, D.R., Byerly, G.R. and Heubeck, C. (2012) *Geologic Map of the West-Central Barberton Greenstone Belt*. Geological Society of America, South Africa.
- Mallik, L., Mazumdar, R. and Mazumdar, B. (2012) Tidal rhythmites in offshore shale: a case study from the Palaeoproterozoic Chaibasa shale, eastern India and implications. *Mar. Pet. Geo.*, **30**(1). <https://doi.org/10.1016/j.marpetgeo.2011.10.005>
- Mazumdar, R. (2001) Quantifying the oldest tidal record: the 3.2 Ga Moodies Group, Barberton Greenstone Belt, South Africa: comment and reply: comment. *Geology*, **29**, 1159.
- Mazumdar, R. (2004) Implications of lunar orbital periodicity from the Chaibasa tidal rhythmites (India) of late Paleoproterozoic age. *Geology*, **32**, 841–844.
- Mazumdar, R. (2005) Proterozoic sedimentation and volcanism in the Singhbhum crustal province, India and their implications. *Sed. Geol.*, **176**, 167–193.
- Meyers, S.R. and Malinverno, A. (2018) Proterozoic Milankovitch cycles and the history of the solar system. *Proc. Natl Acad. Sci. USA*, **115**, 6363–6368.
- Nabhan, S., Luber, T., Scheffler, F. and Heubeck, C. (2016) Climatic and geochemical implications of Archean pedogenic gypsum in the Moodies Group (~3.2 Ga), Barberton Greenstone Belt, South Africa. *Precambrian Res.*, **275**, 119–134.
- Nio, S.D. and Yang, C.H. (1991) Diagnostic attributes of clastic tidal deposits: a review. In: *Clastic Tidal Sedimentology* (Eds Smith, D.G., Reinson, G.F., Zaitlin, B.A. and Rahmani, R.A.), pp. 3–28. Canadian Society of Petroleum Geologists, Calgary, AB.
- Perillo, G.M.E. and Ludwick, J.C. (1984) Geomorphology of a sand wave in lower Chesapeake Bay, Virginia, U.S.A. *Geo Mar. Lett.*, **4**, 105–112.
- Reimann, S., Heubeck, C.E., Fugmann, P., Janse van Rensburg, D.J., Zametzer, A., Serre, S.H. and Thomsen, T.B. (2021) Syndepositional hydrothermalism selectively preserves records of one of the earliest benthic ecosystems, Moodies Group (3.22 Ga), Barberton Greenstone Belt. *South Afr. J. Geol.*, **214**, 253–278.
- Reineck, H.E. and Wunderlich, F. (1968) Classification and origin of flaser and lenticular bedding. *Sedimentology*, **11**, 99–104.
- Richardson, C. (1990) Tidal rhythms in the shell secretion of living bivalves. In: *Earth's Rotation from Eons to Days* (Eds Brosche, P. and Sündermann, J.), pp. 215–226. Springer-Verlag, Berlin.
- Roep, T.B. (1991) Neap-spring cycles in a subrecent tidal channel fill (3665 BP) at Schoorl, NW Netherlands. *Sed. Geol.*, **71**, 213–230.
- Runcorn, S.K. (1979) Palaeontological data on the history of the earth-moon system. *Phys. Earth Planet. Inter.*, **20**, 1–5.
- Schmitz, M. and Heubeck, C. (2021) Constraints on deformation mechanisms of the Barberton Greenstone Belt from regional stratigraphic and structural data of the synorogenic Moodies Group. *Precamb. Res.*, **362**, 106177.
- Smith, D.G., Reinson, G.F., Zaitlin, B.A. and Rahmani, R.A. (Eds.) (1991) *Clastic Tidal Sedimentology*. Canadian Society of Petroleum Geologists, Calgary, AB.
- Sonett, C.P. and Chan, M.A. (1998) Neoproterozoic Earth–Moon dynamics; rework of the 900 Ma Big Cottonwood Canyon tidal laminae. *Geophys. Res. Lett.*, **25**, 539–542.
- Sonett, C.P., Kvale, E.P., Zakharian, A., Chan, M.A. and Dekmo, T.M. (1996) Late Proterozoic and Paleozoic tides, retreat of the Moon, and rotation of the Earth. *Science*, **273**, 100–104.
- Stutenbecker, L., Heubeck, C. and Zeh, A. (2019) The Lomati Delta Complex: a prograding tidal delta in the Archean Moodies Group, Barberton Greenstone Belt. *South Afr. J. Geol.*, **122**, 17–38.

- Sündermann, J. and Brosche, P. (1978) The numerical computation of tidal friction for present and ancient oceans. In: *Tidal Friction and the Earth's Rotation* (Eds Brosche, P. and Sündermann, J.), pp. 125–144. Springer-Verlag, Berlin.
- Toulkeridis, T., Goldstein, S.L., Clauer, N., Kröner, A., Todt, W. and Schidlowski, M. (1998) Sm–Nd, Rb–Sr and Pb–Pb dating of silicic carbonates from the early Archaean Barberton Greenstone Belt, South Africa: evidence for post-depositional isotopic resetting at low temperature. *Precamb. Res.*, **92**, 129–144.
- Trendall, A.F. (1973) Varve cycles in the Weeli Wolli Formation of the Precambrian Hamersley Group, Western Australia. *Econ. Geol.*, **68**, 1089–1097.
- Tyler, R.H. (2021) On the tidal history and future of the earth-moon orbital system. *Planet. Sci.*, **2**, 70. <https://doi.org/10.3847/PSJ/abe53f>
- Vanyo, J.P. and Awramik, S.M. (1985) Stromatolites and Earth-Sun-Moon Dynamics. *Precambrian Res.*, **29**, 121–142.
- Virtanen, P., Gommers, R., Oliphant, T.E., Haberland, M., Reddy, T., Cournapeau, D., Burovski, E., Peterson, P., Weckesser, W., Bright, J., van der Walt, S.J., Brett, M., Wilson, J., Millman, K.J., Mayorov, N., Nelson, A.R.J., Jones, E., Kern, R., Larson, E., Carey, C.J., Polat, I., Feng, Y.U., Moore, E.W., VanderPlas, J., Laxalde, D., Perktold, J., Cimrman, R., Henriksen, I., Quintero, E.A., Harris, C.R., Archibald, A.M., Ribeiro, A.H., Pedregosa, F., van Mulbregt, P., Vijaykumar, A., Bardelli, A.P., Rothberg, A., Hilboll, A., Kloeckner, A., Scopatz, A., Lee, A., Rokem, A., Woods, C.N., Fulton, C., Masson, C., Häggström, C., Fitzgerald, C., Nicholson, D.A., Hagen, D.R., Pasechnik, D.V., Olivetti, E., Martin, E., Wieser, E., Silva, F., Lenders, F., Wilhelm, F., Young, G., Price, G.A., Ingold, G.-L., Allen, G.E., Lee, G.R., Audren, H., Probst, I., Dietrich, J.P., Silterra, J., Webber, J.T., Slavič, J., Nothman, J., Buchner, J., Kulick, J., Schönberger, J.L., de Miranda Cardoso, J.V., Reimer, J., Harrington, J., Rodríguez, J.L.C., Nunez-Iglesias, J., Kuczynski, J., Tritz, K., Thoma, M., Newville, M., Kümmerer, M., Bolingbroke, M., Tartre, M., Pak, M., Smith, N.J., Nowaczyk, N., Shebanov, N., Pavlyk, O., Brodtkorb, P.A., Lee, P., McGibbon, R.T., Feldbauer, R., Lewis, S., Tygier, S., Sievert, S., Vigna, S., Peterson, S., More, S., Pudlik, T., Oshima, T., Pingel, T.J., Robitaille, T.P., Spura, T., Jones, T.R., Cera, T., Leslie, T., Zito, T., Krauss, T., Upadhyay, U., Halchenko, Y.O. and Vázquez-Baeza, Y. (2020) SciPy 1.0: Fundamental algorithms for scientific computing in Python. *Nat. Methods*, **17**, 261–272.
- Visser, D.J.L. (comp., with reports by Eeden, O.R. van, Joubert, G.K., Söhnge, A.P.G., Zyl, J.S. van, Rossouw, J., Taljaard, J.J., and Visser, D.J.L.). (1956) The geology of the Barberton area. *Geological Survey of South Africa Special Publication* **15**, 253 p.
- Visser, M.J. (1980) Neap-spring cycles reflected in Holocene subtidal large-scale bedform deposits: a preliminary note. *Geology*, **8**, 543–546.
- Webb, D.J. (1982) Tides and the evolution of the Earth—Moon system. *Geophys. J. Roy. Astron. Soc.*, **70**, 261–271.
- Wever, T.F. and Stender, I.H. (2000) Strategies for and results from the Investigation of Migrating Bedforms in the German Bight. Proceedings of the International Workshop “Marine Sandwave Dynamics”, Lille, France, 2000.
- Williams, G.E. (1990) Tidal rhythmites: key to the history of the Earth's rotation and the lunar orbit. *J. Phys. Earth*, **38**, 475–491.
- Williams, G.E. (1991) Upper Proterozoic tidal rhythmites, South Australia: sedimentary features, deposition, and implications for the earth's rotation. In: *Clastic Tidal Sedimentology* (Eds Smith, D.G., Reinson, G.E., Zaitlin, B.A. and Rahmani, R.A.), *Can. Soc. Pet. Geol. Mem.*, **16**, 161–178.
- Williams, G.E. (2000) Geological constraints on the Precambrian history of Earth's rotation and the Moon's orbit. *Rev. Geophys.*, **38**, 37–59.
- Williams, G.E. (2004) Earth's Precambrian rotation and the evolving lunar orbit: implications of tidal rhythmite data for palaeogeophysics. In: *The Precambrian Earth—Tempos and Events Developments in Precambrian Geology* (Eds Eriksson, P.G., Altermann, W., Nelson, D., Mueller, W., Cateneau, O. and Strand, K.), Vol. **12**, pp. 473–482. Elsevier, Amsterdam.
- Williams, G.E. (2005) Comment on “Tidal rhythmites and their implications” by R. Mazumder and M. Arima [Earth-Science Reviews, 69 (2005) 79–95]. *Earth Sci. Rev.*, **72**, 113–117.
- de Wit, M.J. and Ashwal, L.D. (1995) Greenstone belts - what are they? *S. Afr. J. Geol.*, **98**, 505–520.
- Xie, X., Byerly, G.R. and Ferrell, R.E. (1997) Ilb trioctahedral chlorite from the Barberton greenstone belt: crystal structure and rock composition constraints with implications for geothermometry. *Contrib. Mineral. Petrol.*, **126**, 275–291.
- Yang, C.S. and Nio, S.D. (1985) The estimation of Palaeohydrodynamic processes from subtidal deposits using time series analysis methods. *Sedimentology*, **32**, 41–57.
- Zeh, A., Gerdes, A. and Heubeck, C. (2013) U-Pb and Hf isotope data of detrital zircons from the Barberton Greenstone Belt: constraints on provenance and Archaean crustal evolution. *J. Geol. Soc.*, **170**, 215–223.
- Zeiler, M., Schulz-Ohlberg, J. and Figge, K. (2000) Mobile sand deposits and shore-face sediment dynamics in the inner German Bight (North Sea). *Mar. Geol.*, **170**, 363–380.

Manuscript received 26 May 2021; revision accepted 22 February 2022